Nigerian Journal of Theoretical and Environmental Physics (NJTEP)
ISSN Print: 3026-9601
DOI: https://doi.org/10.62292/njtep.v2i1.2024.1
Volume 2(1), March 2024

Groundwater Protection Assessment using Frequency Domain Electromagnetic Method and Direct Current Electrical Resistivity Method in Papalanto South-West Nigeria

Ishola, S. A.

Department of Earth Sciences, Olabisi Onabanjo University Ago-Iwoye, P.M.B 2002, Ago-Iwoye, Ogun State, Nigeria

*Corresponding author's email: ishola.sakirudeen@oouagoiwoye.edu.ng

ABSTRACT

The aim of this work is to assess the extent of protection of the subsurface hydrogeological structures. Fieldworks were performed integrated geophysical techniques namely Frequency Domain Electromagnetic Method (FDEM) using Geonics-EM-34 to determine the vertical and lateral variations of subsurface conductivity probing depths of 20m, 40m and 60m, while subsurface profiles were obtained using Direct Current Resistivity (DCRE) with AGI Super-sting Earth Resistivity meter; current electrode spacing (AB) ranging from 1 to maximum of 100m and the potential electrodes (MN) were consequently changed from 0.25m to 5m respectively. 1141.92 mmho/m was recorded as the highest true conductivity value for the Horizontal Dipole in the second layer (Profile EMPAP5) while the highest true conductivity value for the Vertical Dipole in the first layer was 134.31 mmho/m (Profile EMPAP1). Four principal geoelectric layers inferred from the VES data where the Topsoil is partly lateritic and alluvium, Sandy Clay/Clay/Silt, Sand/Clay/Shale, and Limestone/Sandstone. Resistivity values for these layers vary from 9.78 to 1428, 1.46 to 1057, 1.46 to 451, and 15 to 10,000 Ω m with corresponding thickness of 0.5m to1.43m, 1.29m to 13m, 2.8m to 84.4m and infinity, respectively. The higher resistivity values at the surface and extremes of both edges were indication of little or no presence of leachates or contaminant plume accumulation in other area. Also, there was a noticeable general decrease of resistivity values of formation rock with depth in these investigated areas; this is an indication that the plumes must have infiltrated rapidly into the subsurface through the massive presence of weathered rock materials of average lateral distances of 15m to 167m of considerable depth and thickness of about 24.9m. The degree of leachate contamination range from 0.0007264 mho to 0.668 mho with the highest value in VESPAP2 followed by VESPAP13 and VESPAP19 while VESPAP22 exhibited the lowest conductance.

Keywords:
Leachate,
Vulnerability,
Resistivity,
Tomography,
Protective capacity.

INTRODUCTION

Daily infiltration of rainfall into the subsurface and landfill together alongside the biochemical breakdown of the wastes produces leachate which is high in suspended solids and possesses varying organic and inorganic contents. Once these leachates enter the subsurface or groundwater environment before sufficient dilution occurs, serious contamination incidents would transpire (Desa et al., 2009). The application of geophysical methods for groundwater assessment and hydrogeological site characterization has increased in the last decade (Vereecken et al., 2004; Herckenrath et al., 2013; Ishola et al., 2021). Several authors have applied geophysical methods to solve hydrogeological related problems (Faneca Sànchez et al., 2012; Burschil et al., 2012). Leachate plumes have been found to be more electrically conductive than the surrounding pore waters in the subsurface environment which are often detected by appropriate geophysical electrical geophysical methods notably electromagnetic method, electrical resistivity method and self/induced potential method (Bayode et al., 2011; Ayolabi et al., 2013; Ishola et al., 2021). Frequency domain electromagnetic method is often and widely used to map near surface geology and for determining the subsurface conductivity status while outlining shallow conductive

hydrogeological structures probably connected with local water circulation (Ishola et al., 2021). The results of such a study are also important in the future delimitation of a protected zone from contamination and have been successfully applied in varying groundwater and environmental conditions to locate zones. The electrical resistivity method is most frequently used in environmental studies because the electrical resistivity of earth materials is determined by parameters such as fluids, conductivity of the matrix, porosity, permeability, temperature, degree of fracturing, grain size, degree of cementation, rock type and the extent of weathering of the medium (Olorunfemi, 2001; Idornigie et al., 2006).

The study area is prone to varying activities which makes it vulnerable to effluents discharges, wastes infiltrating the substrate and possibly find its way into groundwater aquifers, Slurries and liquefied wastes are possible source of leachate contamination in the study area while the common tailings found in the study area include papers, sack bags, used plastic, rubbers and debris of wood and cement dusts (WAPCO, 2000; Ishola, 2019). According to published report, Nigeria as a country generates an average of 0.58 kg solid waste per person daily (Adewumi et al., 2005) with a population of over 170 million people; this huge figure if left uncontrolled would inadvertently lead to serious environmental problems that might be very difficult to remediate. Hence, it is imperative to provide a proper assessment cum understanding of the environmental hazards possibly associated with indiscriminate, unguided and open waste disposal practices. This study focuses on availability of geological barriers to groundwater pollution and vulnerability of aquifer to leachate contamination in Papalanto, Southwestern Nigeria. This paper starts with a succinct introduction to the case study area, the suitability of the electrical method for this investigation, and a discussion on the role of lithology at impeding the flow of leachate in the subsurface. This work is basically a geophysical approach to the interpretation of the leachate and does not include coring or sampling for geochemical analysis purposes.

MATERIALS AND METHODS

The Study Areas

Location and Accessibility

Papalanto area is approximately bounded by longitude $3^{0}13^{1}$E and $6^{0}54^{1}$N and harbours one of the largest outcrops of Ewekoro limestone that easily attracts attention. It extends from Ibesse, 4km east of Papalanto along Papalanto-Shagamu road to Ogun River, 5km east to Iro community. The Ewekoro formation at the type locality is composed of 11m to 12m of limestone. It is sandy at the base grading downward into Abeokuta Formation. The Ewekoro formation is overlain of phosphatic glauconitic grey shale (Jones and Hockey, 1964). It occupies a total area of 16,400 $km^2$with a population of 255,156 at 2006 population Census and a postal code area of 112 with an average elevation of 64m above sea level. The area is mildly densely populated with 297 people per Km^2 with the nearest town larger than 50,000 inhabitants takes about 0:15 hour by local transportation. An estimated 2.5% of the children are underweight with a notably of 100 per 1000 births. The indigenous dwellers of Ewekoro Local Government area are mainly the Egbas, particular the Egba Owus. The people engage primarily in farming and trading activities. The area is essentially in rural settlement (Ishola, 2019). The climate is not different from that of these towns and villages earlier mentioned and adjoining towns such as Ifo, Sagamu and others (Ishola, 2019). Fig. 1 shows the Geological Map of the Selected Locations of the Study Area within the Nigerian Part of Dahomey Embayment (Billman, 1992; Ishola, 2019), Fig. 2 Displays the GoogleEarth imagery of the selected Investigated study area within in Ewekoro LGA, Southwest Nigeria, Fig. 3 is a the map of the investigated locations in the study area.

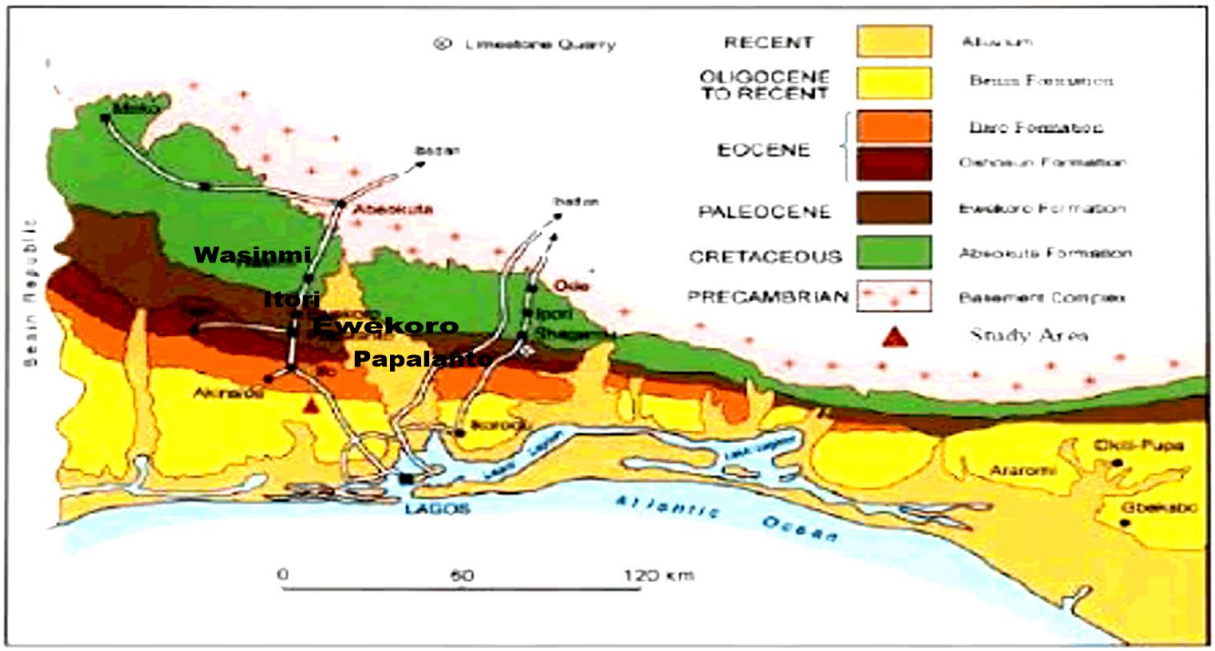

Figure 1: Geological Map Showing the Selected Locations of the Study Area within the Nigerian Part of Dahomey Embayment (Billman, 1992; modified by Ishola, 2019).

Figure 2: Display of GoogleEarth imagery of the selected Investigated study area within in Ewekoro LGA, Southwest Nigeria (Ishola, 2019)..

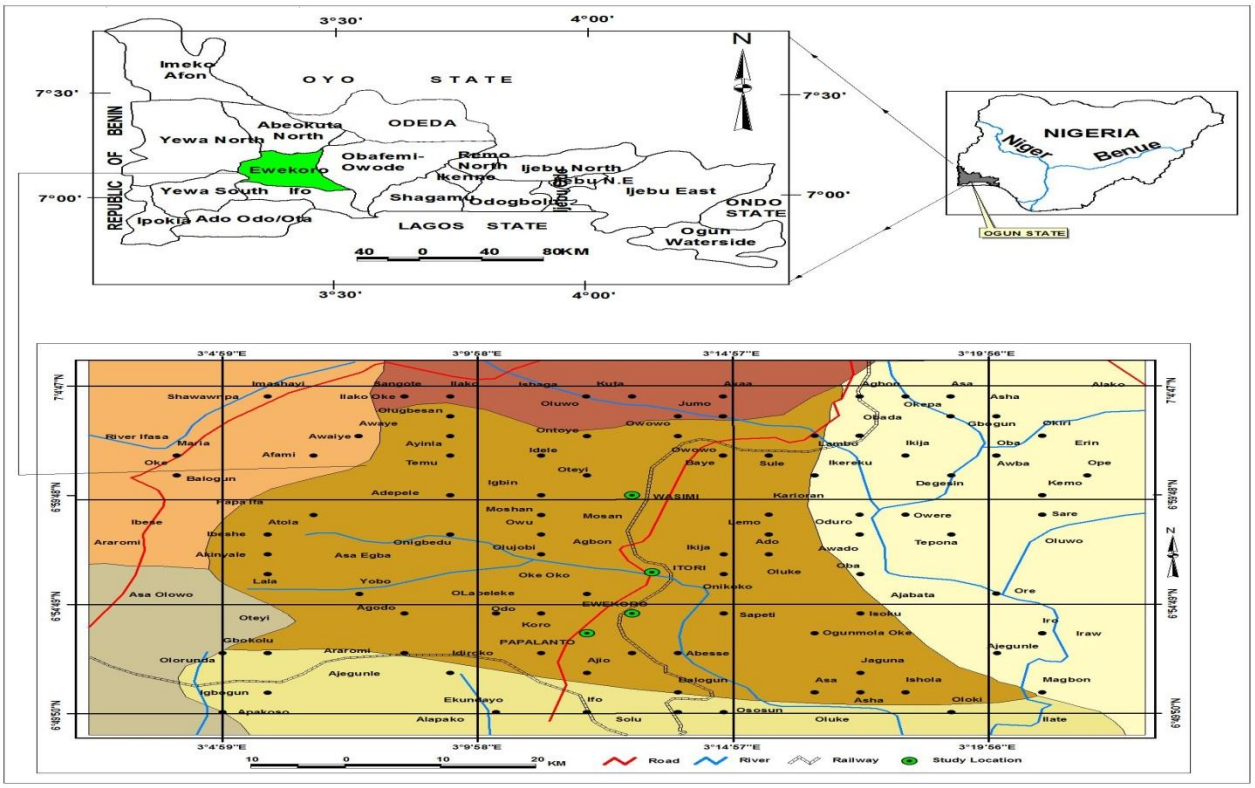

Figure 3: Inset Map showing the Study Areas in Ogun State within Nigeria Continental Domain (Arcview GIS 3.2A Environment) (Ishola, 2019)

Theoretical Background and Principle of Operations

Electromagnetic method makes use of a response of the ground to the propagation of electromagnetic fields which are composed of an alternating electric intensity and magnetizing force. Electromagnetic method does not require contact with the ground, therefore the speed with which EM can be made is much greater than the electrical method. An electromagnetic field can be generated by passing an alternating current through either a small coil comprising many turns of wire or a large loop of wire (Ishola, 2019).

An electromagnetic field may be defined in terms of vector E, D, B, where:

E is the electrical field in V/m., D is the dielectric displacement in Coulomb/m².

H is the magnetic field intensity in A/m., B is the magnetic induction in Tesla.

Maxwell's equations using Faraday's law

Experimental evidence shows that all electromagnetic phenomena obey the following four Maxwell equations.

$$\nabla E = -\frac{\partial B}{\partial t} \quad (1)$$

Faraday's law shows us how a time varying magnetic field produces an electrical voltage.

Maxwell's equations using Ampere's law

Ampere's law shows us how an electric current and/or a time varying electric field generate a magnetic field.

$$\nabla H = J + \frac{\partial D}{\partial t} \quad (2)$$

Maxwell's Equations infer that lines of magnetic induction are continuous and there are no single magnetic poles (Ishola, 2019).

$$\text{div } B = 0 \quad (3)$$

It infers that electrical fields can begin and end on electrical charges.

$$\text{div } D = q \quad (4)$$

Subsidiary equations and wave equation

By using the following subsidiary equations,

$$D = \epsilon E, \quad B = \mu H, \quad J = \sigma E \quad (5)$$

Where J is the electrical current density in A/m²; q, the electric charge in Coulomb/m³; ϵ, the electrical permittivitiy; μ, the magnetic permeability and σ $r$epresents the electrical conductivity

From these four Maxwell equations the electromagnetic wave equation can be derived.

Primary and Secondary Fields

Where the subsurface is homogeneous there is no difference between the fields propagated above the surface and through the ground (only slight reduction in amplitude). If a conductive anomaly is present, the

magnetic component of the incident EM wave induces alternating currents (Eddy currents) within the conductor (Fig. 4); the eddy currents generate their own secondary EM-field which travels to the receiver. The receiver also detects the primary field which travels through the air. The receiver responds then to the resultant of the arriving primary and secondary fields. Consequently, the measured response will differ in both phase and amplitude relative to the unmodulated primary field (Ishola, 2019). These differences between the transmitted and received electromagnetic fields reveal the presence of the conductor and provide information on its geometry and electrical properties. The depth of penetration of an electromagnetic field depends upon the frequency and electrical conductivity of the medium through which it is propagating. Electromagnetic fields are attenuated during their passage through the ground**.** The amplitude of EM fields decreases exponentially with depth. The amplitude of EM-radiation as a function of depth relative to its original amplitude A_0 is given by

$$A_d = A_0 e^{-1}. \quad (6)$$

The depth of penetration d can be defined as the depth at which the amplitude of the field A_d is decreased by the factor e^{-1} compared with its surface amplitude A_0 (Ishola, 2019). Penetration depth d is given by

$$d = \frac{503.8}{\sqrt{\sigma f}} \quad (7)$$

where d is in metres, the conductivity s of the ground is in Sm^{-1} and the frequency of the field is in Hz.

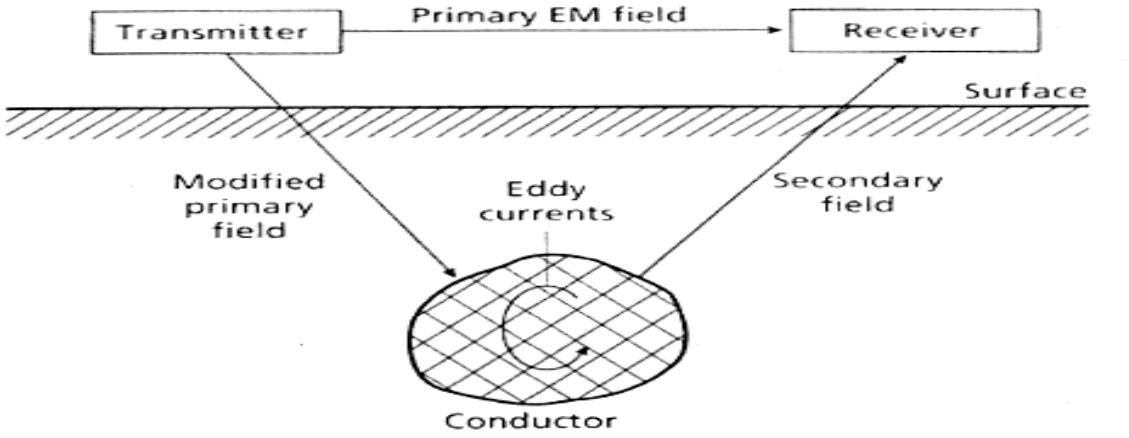

Figure 4: General Principle of Electromagnetic Surveying (Vogelsang, 1995)

The depth of penetration thus increases as both the frequency of the electromagnetic field and the conductivity of the ground decrease. Consequently, the frequency used in an EM survey can be tuned to a desired depth range in any particular medium where equation (7) represents a theoretical relationship. Empirically, an effective depth of penetration z_e can be defined as the depth which represents the maximum depth at which a conductor may lie and still produce a recognizable electromagnetic anomaly (Ishola, 2019).

$$z_e = \frac{100}{\sqrt{\sigma f}} \quad (8)$$

The relationship is approximate as the penetration depends upon such factors as the nature and magnitude of the effects of near-surface variations in conductivity, the geometry of the subsurface conductor and instrumental noise. The frequency dependence of the depth of penetration places constraints on the EM method. Normally, very low frequencies are difficult to generate and measure and the maximum achievable penetration is usually of the order of 500m (McNeil, 1980; Keary *et al.,* 2002; Omosuyi et al., 2007; Ishola, 2019). Examples of different Depths of penetration and corresponding frequencies for 10m spacing are f = 10Hz, d =503m; f =100Hz, d = 159m and f = 1000Hz, d = 50.3m.

EM 34-3 Basis, Principle of Operation and Interpretation Technique

The Electromagnetic Ground Conductivity Survey Method used is based on a well established surface geophysical method. The instrument used was the EM 34-3 terrain conductivity meter by Geonics Ltd obtained from the Department of Geosciences, University of Lagos. A change in conductivity of 5 mS/cm was assumed to be measurable with the instrument which provides a direct reading of the apparent conductivity (σ_a) of the ground in units of millimhos per metre (SI equivalent units are millisiemens per metre (mS/m)). The ratio of the intercoil spacing (s) divided by the skin depth (δ) is known as the induction number (Ishola *et al*., 2021).

In FDEM method, HD/VD surveys were carried out using a GEONICS EM-34 meter has separate coils connected by a reference cable provide the basis of the system, which can be 10m, 20m and 40 m long. The

effective depth investigations are 7.5 m (HD) and 15 m (VD) for a frequency of 6.4 KHz and separation of 10 m. For a separation of 20 m and frequency of 1.6 Hz, is obtained a depth investigation of 15 m (HD) and 30 m (VD), as soon as, for the separation of 40 m and frequency of 0.4 Hz, the investigation (GEONICS, 1990; Ishola *et al.*, 2021).

Ground Conductivity (Measurements at Low Induction Number)

The instrument (manufactured by Geonics Ltd.) provides a direct reading of the quadrature as the apparent conductivity in mS/m. Consequently, the secondary magnetic field is a complicated function of the inter-coil spacing, (s), the operating frequency (f), and the ground conductivity (σ). However, However, under certain constraints technically defined as "operation at low values of induction number" the secondary magnetic field is a very simple function of these variables incorporated in the design of the EM 34-3 (McNeill, 1980b). It can be shown that if the product of s and the skin depth d, known as the induction number, is much less than unity. Therefore, the ratio of the intercoil spacing (s) divided by the skin depth is known as the induction number B where the induction number is less than one, then the ratio of the secondary to the primary of magnetic fields at the receiver is directly proportional to apparent conductivity.

The ratio of the secondary (H_s) to primary (H_p) magnetic fields at the receiver at low induction n umbers (B<<1) is given by

$$\frac{H_s}{H_p} = \frac{i\omega\mu_B\sigma s^2}{4} \quad (9)$$

The apparent conductivity indicated by the instrument is deduced from equation (9) as:

$$\boldsymbol{\sigma} = \frac{\mathbf{4}}{\boldsymbol{\omega\mu_B s^2}}\left(\frac{H_s}{H_p}\right) \quad (10)$$

Where H_s is the amplitude of the secondary electromagnetic field at the receiver coil; H_p, the amplitude of the primary electromagnetic field at the receiver coil; ω, the angular frequency ($\omega = 2\pi f$); f, the frequency (Hertz); μ_B, the magnetic permeability of vaccum or free space (1.2566×10^{-6} m kg C^{-2}); σ, ground conductivity (mho/m); s, the inter coil spacing (m) and *i* is the parameter indicating the presence of a quadrature component (Ishola, 2019).

Thus the ratio of H_s/H_p is proportional to the ground conductivity σ. Since depth d depends on the product of estimation of the maximum probable value of σ allows the selection of f such that the above condition of low induction number is satisfied. The depth of penetration depends upon σ and is independent of the conductivity distribution of the subsurface. Measurements taken at low induction number thus provide an apparent σ_a given by

$$\boldsymbol{\sigma}_a = \frac{1}{\rho_a} = \frac{\mathbf{4}}{\boldsymbol{\omega\mu_B s^2}}\left(\frac{H_s}{H_p}\right)q \quad (11)$$

This relationship allows the construction of elecromagnetic instruments which provide a direct reading of ground conductivity down to predetermined depth. The measuring system is designed to ensure that with the selected frequency f, for a given inter-coil separation (s), a designed response of H_p for a given transmitter, the only unknown H_s which is measured by the instrument where the subscript q denotes the quadrature phase (Ishola, 2019).

To measure the terrain conductivity the search coil is either held horizontally (measurement in vertical dipole mode) or vertically (measurement in horizontal dipole mode). The results are generally shown in the form of profiles as inductive electromagnetic survey methods are, nowadays, widely used to map near-surface geology by mapping variations in the electrical conductivity of the ground. Such variations generally are caused by changes in soil structure, porosity, clay content, resistivity of the soil water, and degree of water-saturation in the soil (GEONICS, 1990; Ishola, 2019).

Data Processing, Inversion and Analysis

The EM data was qualitatively checked by observing if negative apparent conductivity was recorded. Field note was used as a guide to identify if some anomalously high apparent conductivity values are due to artifacts. The apparent conductivity reading of the horizontal dipole orientation on each traverse was plotted against station midpoint. This was also carried out separately for the vertical dipole orientation. The crossplots of apparent conductivity on the different spacing enabled a view of how the conductivity varies with depth. Qualitative analysis and interpretation was carried out on the plotted data.

The electrical resistivity data was downloaded from the automated system in stg. Format and can be viewed with notepad. The data was processed for bad data points such as negative resistivity before inversion was carried out. Both processing and inversion were carried out with Earth Imager. The software plots the field or measured data pseudosection and generates a calculated or theoretical model. It then carries out inversion by comparing both the measured and calculated model to generate an inverted model which is a representative of the true subsurface resistivity at different depth investigated. Interpretation of the VES data was done by partial curve matching from which a resistivity and depth model is derived (Fig. 4). This field-derived apparent resistivity data was the principal input for computer iteration in WINRESIST software (Vander Velpen, 1988). The final resistivity values provided 1D dimensional information about the earth (Omosanya et al., 2014). Resistivity and thickness values were later interpolated to cross sections through the study area.

The subsurface resistivity of the area is compared to the similar resistivity values from boreholes in Itori and Ewekoro which have similar geology to the study area and to standard resistivity chart of Palacky, 1988. The derived pseudosection were inverted, a process that allows the apparent resistivity to be plotted against the true depth rather than electrode spacing. The results obtained from the pseudosection were further interpreted by describing the resistivity of each layer as compared with the standard resistivity of rock types (Palacky, 1988, Nton, 2001; Akinmosin et al., 2013; Ishola, 2019).

The AVI Method

Another method of aquifer vulnerability assessment is the Aquifer Vulnerability Index (AVI) of Van Stempvoort *et al.*, (1993). This method was approved by the Canadian Prairie Provinces Water Board. The AVI methodological strength relies on vadose zone characterisation which has been noted as being the most important single parameter in aquifer vulnerability evaluation (McLay *et al.*, 2001; Herbst *et al.*, 2005). It can be directly related to the physical properties of the vadose zone (Ross *et al.*, 2004). The AVI computes aquifer vulnerability on the basis of the hydraulic resistance (c), as a ratio between the thickness of each sedimentary unit above the uppermost aquifer (d), and the estimated hydraulic conductivity of each of these layers (K). Hydraulic resistance is calculated by:

$$c = \sum_{i=1}^{n} \frac{d_i}{K_i} \quad (12)$$

Where n is the number of sedimentary units above the aquifer, d_i, thickness of the vadose zone;

K_i = hydraulic conductivity of each protective layer; K, unit of length/time (m/s or m/d)

c, travel time with dimension in seconds

The hydraulic resistance c (vulnerability index) is an inverse indicator of vulnerability: This is vertical flow of water through the protective layers. This can be used as a rough estimate of vertical travel time of water through the unsaturated layers. It is important to note that significant parameters controlling the travel time like hydraulic gradient and diffusion are not considered in AVI. Even if there are a lot of methodologies that consider the processes occurring in the vadose zone more accurately, the AVI method is one of the best (Lasserre *et al.*, 1999; Connell and Daele, 2003). The AVI index is perhaps most suitable at a large regional scale vulnerability assessment (Zwahlen, 2004).

Weaknesses of the AVI Method

The AVI method is not regarded as a complete vulnerability method; the c is hydraulic resistance of fluid and not the only factor resisting fluid movements; the method is too simplified (Van Stempvoort *et al.*, 1992). The state of leachate contamination was tested using parameters such as aquifer vulnerability index, overburden protective capacity and longitudinal unit conductance (S*i*) derived from the apparent resistivity values. The apparent resistivity values were used to calculate parameters such as aquifer vulnerability index (AVI) and overburden protective capacity (Van Stempvoort *et al.*,1992; (Ishola, 2019). The protective capacity of groundwater aquifers is a function of the covering layers usually referred to as the protective layers (Kirsch, 2006). Surface water percolates through the protective layers leading to groundwater recharge. During this percolation process, contaminant degradation can occur by mechanical, physicochemical, and microbiological processes. An effective groundwater protection is given by protective layers with sufficient thickness and low hydraulic conductivity leading to high residence time of percolating water. The aquifer vulnerability index (AVI) quantifies aquifer vulnerability by hydraulic resistance which is a function of thickness and hydraulic conductivity of each protective layer to vertical flow of water. Typical values for hydraulic conductivity were based on Freeze and Cherry (1979). Van Stempvoort *et al.*,1992) subsequently classified aquifers with high hydraulic resistance with low vulnerability to contamination.

Furthermore, the overburden protective capacity in the area was evaluated using longitudinal unit conductance (S*i*) derived from the first-order parameters obtained from the VES results (Henriet 1976; Oladapo *et al.*, 2004).

RESULTS AND DISCUSSION

EM Field Data Processing and Interpretation

The electromagnetic data acquired in the field were plotted in arithmetic graph as the peaks (conductivity anomaly) were used as the spot areas for the VES profile. The horizontal and vertical coil data (in milli siemens/meter) were plotted on the same scale against the station intervals (in meters). The plots of horizontal and vertical coils measured in the field are presented as conductivity profiles of the EM data as displayed in Fig. 5a to Fig. 5j. The EM anomalies vary significantly; some are sharp while others are broad (Omosuyi *et al.*, 2008). Zones with peak inflexion were inferred conductive, typical of water filled zones and/or fractures (Ugwu and Nwosu, 2009) or effects of appreciable weathering.

In Papalanto study locations, five traverses were created with the station intervals of 500m. The length of each traverse ranged from 150m to 200m. Three traverses were established in the West and the East trending the North-South direction and two traverses to the North and South in the NW-SE direction. On each traverse, the first Profile was created in the W-E direction and second Profile created in the N-S direction with both Profiles having a Profile length of 200m.

Electromagnetic Profiling along Papalanto traverse 1 and 2 (EMT_1)

Fig. 5a and Fig. 5b shows the Apparent Conductivity Profiles (EMPAP1 and EMPAP2) along the first traverse EMT_1 conducted in the West and runs across the NW-SE direction of Papalanto study area at 10m, 20m and 40m seeking different investigation depths.

The traverse displays appreciable variation in conductivity except a distance of about 20m to 120m in Profile EMPAP1 and 20 m to 150 m in Profile EMPAP2 where there are few recognizable positive peaks and broad anomalies of about 191 mmho/m, 284 mmho/m, 134mmho/m, 200 mmho/m, 198 mmho/m and 168 mmho/m which could be as a result of weathering of the subsurface geological horizon in the study locations. These locations could be inferred as zones of interest for current and future groundwater exploitation and consequently described as weathered to highly weathered/fractured zones which may serve as suitable aquiferous regions for water supply needs of the study area (MacDonald *et al.,* 2005).

The calculated true conductivity values of 118 mS/m and 133.33 mS/m with the corresponding depth values of 9m and 14m recorded for both horizontal and vertical dipole orientations for the first layer while the conductivity values of 138 mS/m and 134.31 mS/m were recorded for the second layer in Profile EMPAP1.Also, the calculated true conductivity values of 122mS/m and 116mS/m with the corresponding depth values of 4.3 m and 114 m were recorded for both the horizontal and vertical dipole orientations for the first layer while the conductivity values of 127 mS/m and 121.88 mS/m were recorded for the second layer in EMPAP2. The high conductivity observed on both Profiles is indicative of possible invasions of the subsurface by contaminant plumes; the contaminant plumes is associated to leachates or contaminant seepages emanating from the exotic and decaying materials from the surface percolating through the overlying layers of rock formations to the subsurface. The results of the horizontal and vertical dipole orientations on both Profiles are slightly correlative with small variation shown in the plots. The high conductivity values (65 mmho/m−284 mmho/m in traverse 1) notably within the lateral extension of 80 m to 130 m and (44 mmho/m-222 mmho/m) in traverse 2 within the lateral distance of 50 m to 120 m by both the horizontal and vertical dipole orientations on both profiles are indicative of the vulnerability of its hydrogeological environment to invasion of contaminant seepages and consequently possible pollution of the investigated locations of the study area.

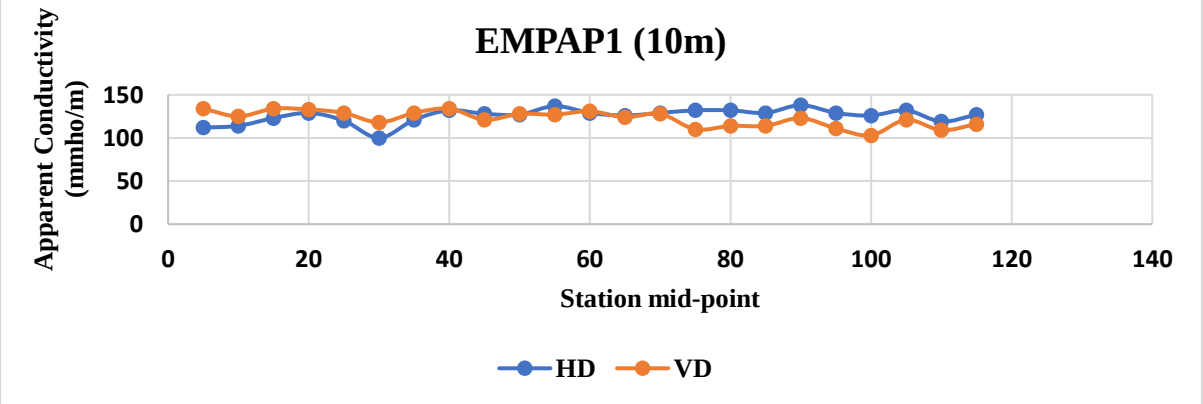

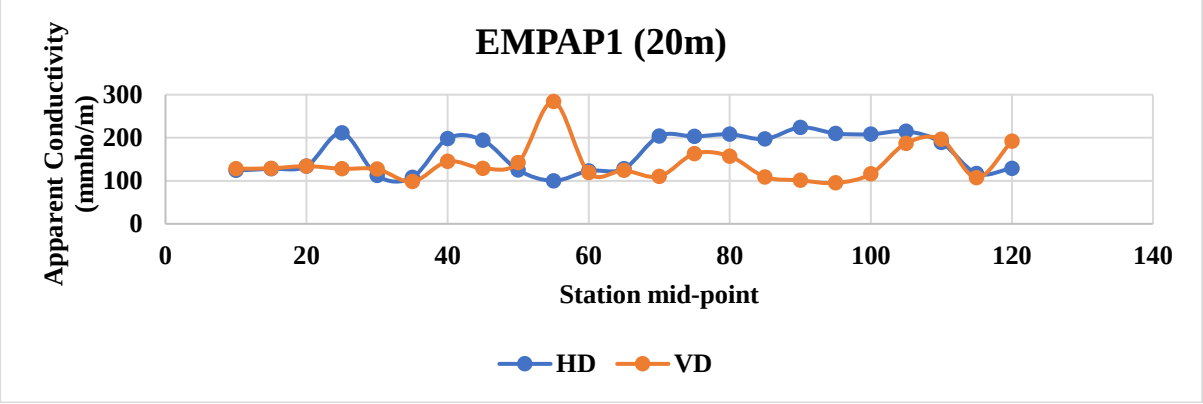

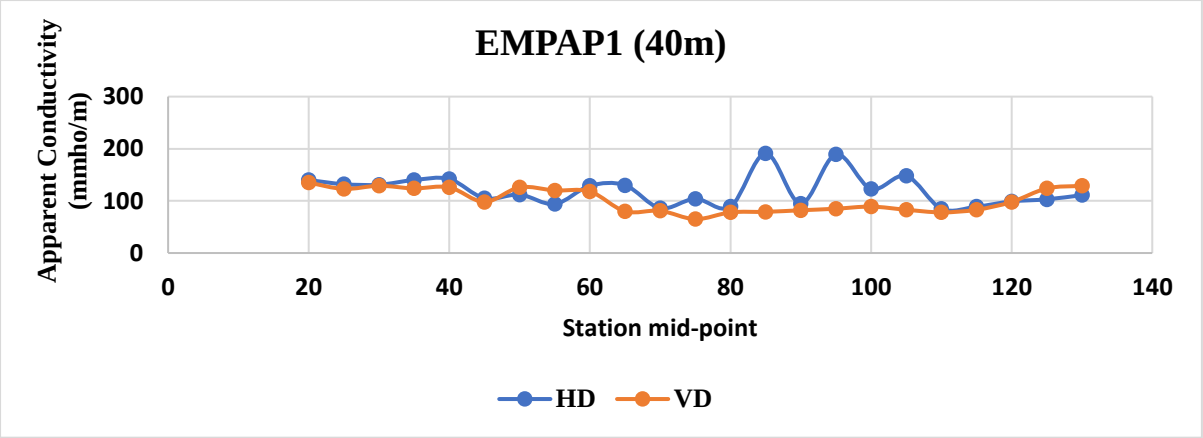

	True Conductivity (mS/m)		Depth(m)	
	HD	VD	HD	VD
1st Layer	118	133.33	9	14
2nd Layer	138	134.31	-	-

Figure 5a: Plot and Values of Apparent and Real Conductivity of Horizontal Dipole Orientations along Papalanto Traverse 1 (Profile 1)

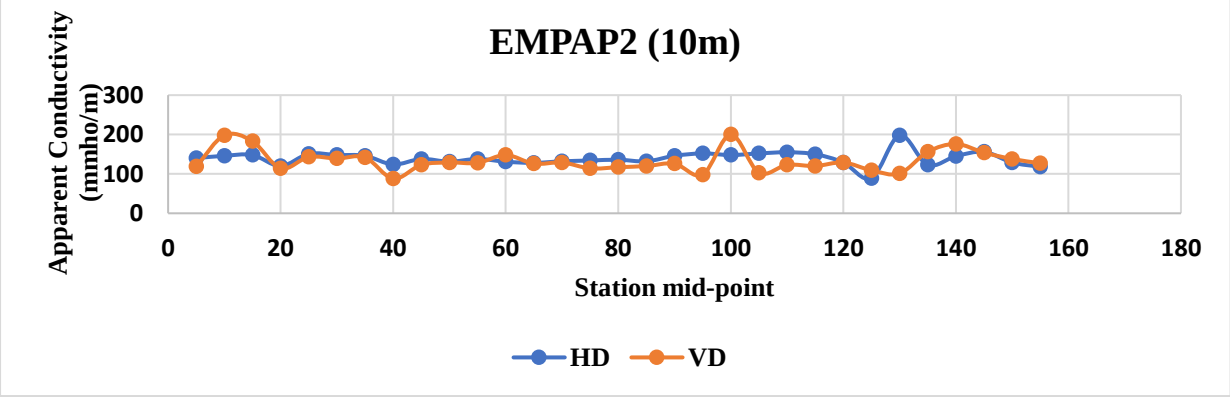

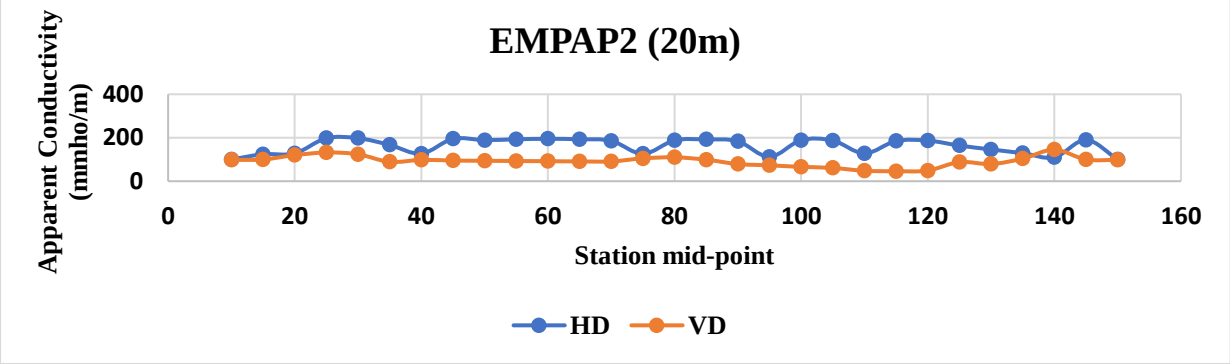

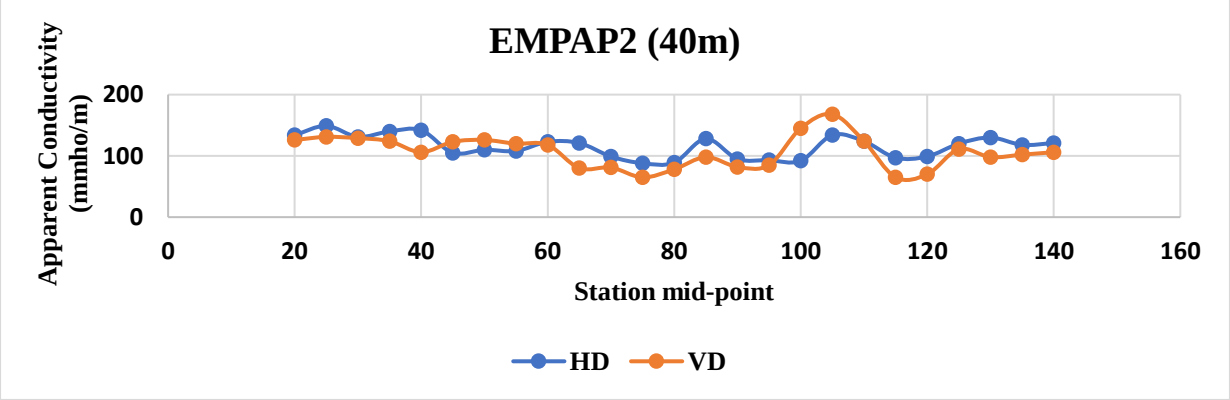

	True Conductivity (mS/m)		Depth (m)	
	HD	VD	HD	VD
1st Layer	122	116	4.3	14
2nd Layer	127	121.88	-	-

Figure 5b: Plot and Values of Apparent and Real Conductivity of Horizontal Dipole Orientations along Papalanto Traverse 1 (Profile 2)

Electromagnetic Profiling along Papalanto traverse 2 (EMT_2)

Fig. 5c and Fig. 5d shows the Apparent Conductivity Profiles (EMPAP3 and EMPAP4) along the second traverse EMT_2 conducted in the West and runs across the NW-SE direction of Papalanto study area at 10m, 20m and 40m seeking different investigation depths.

The traverse displays appreciable variation in conductivity except a distance of about 50m to 200m in Profile EMPAP3 and 50 m to 150 m in Profile EMPAP4 where there are few recognizable positive peaks and broad anomalies of about 189 mmho/m, 222 mmho/m, 172 mmho/m, 172 mmho/m, 216 mmho/m and 178 mmho/m which could be as a result of the weathering of the subsurface geologic formation of the study locations.

These locations could be inferred as zones of interest for possible groundwater recharge and exploitation and consequently described as weathered to highly weathered/fractured zones which may serve as suitable aquifer for local water supply of the study area (MacDonald *et al.*, 2005). The observed varying degrees of conductivity values were delineated as presented in the plots with the most conductive area having conductivity value of 222 mmho/m and the least conductive area having a conductivity value of 44mmho/m respectively inferred as conductive and resistive zones. Consequently, vertical electric sounding of VESPAP6, VESPAP7 and VESPAP8 were conducted in Profile EMPAP3 while VESPAP9 and VESPAP10 were conducted in Profile in Profile EMPAP4 in order to investigate and ascertain the possible depth as well as to infer the geoelectric lithology of the surveyed area due to the observable and significant positive changes in conductivity depicting target zones of appreciable low resistivity suspected of a typical water saturated hydrogeologic unit of fractured zone

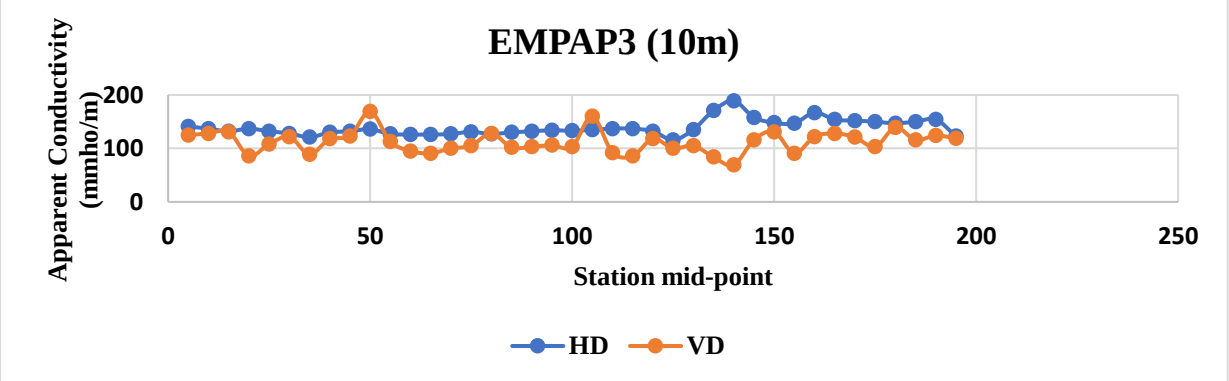

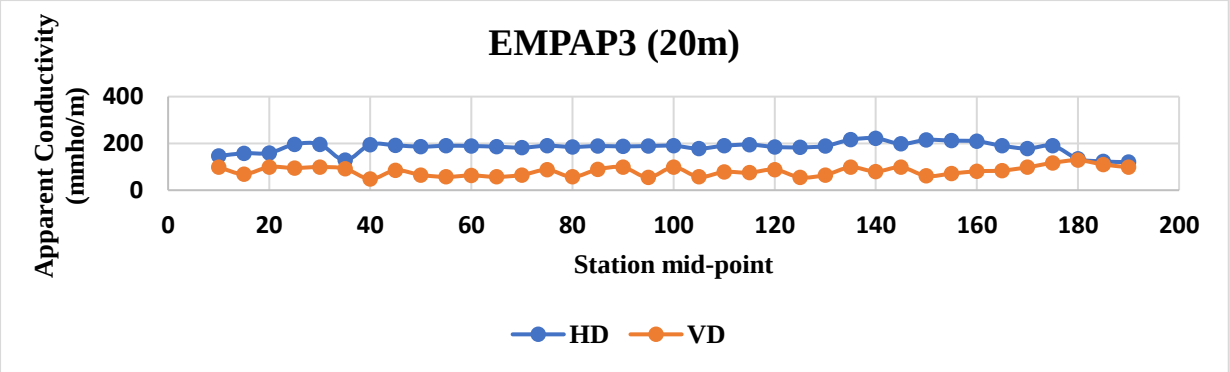

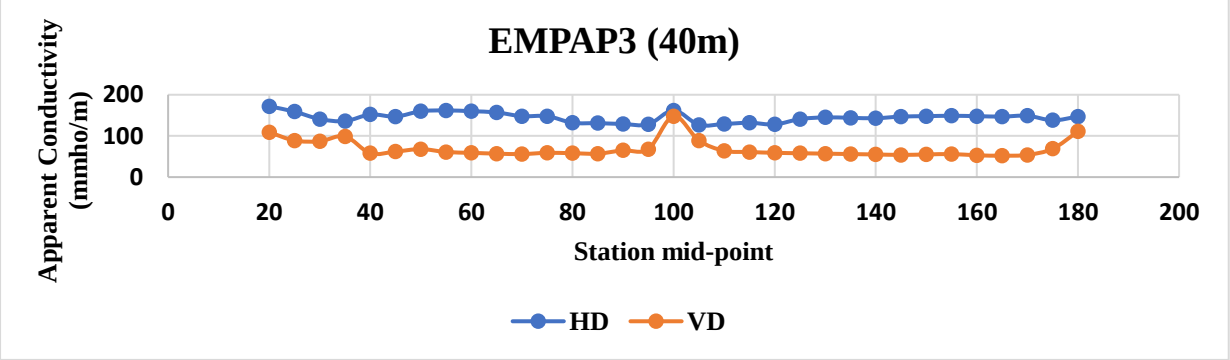

	True Conductivity (mS/m)		Depth (m)	
	HD	**VD**	**HD**	**VD**
1st Layer	146	90	2	9.8
2nd Layer	151.2	100	-	-

Figure 5c: Plot and Values of Apparent and Real Conductivity of Horizontal Dipole Orientations along Papalanto Traverse 2 (Profile 3)

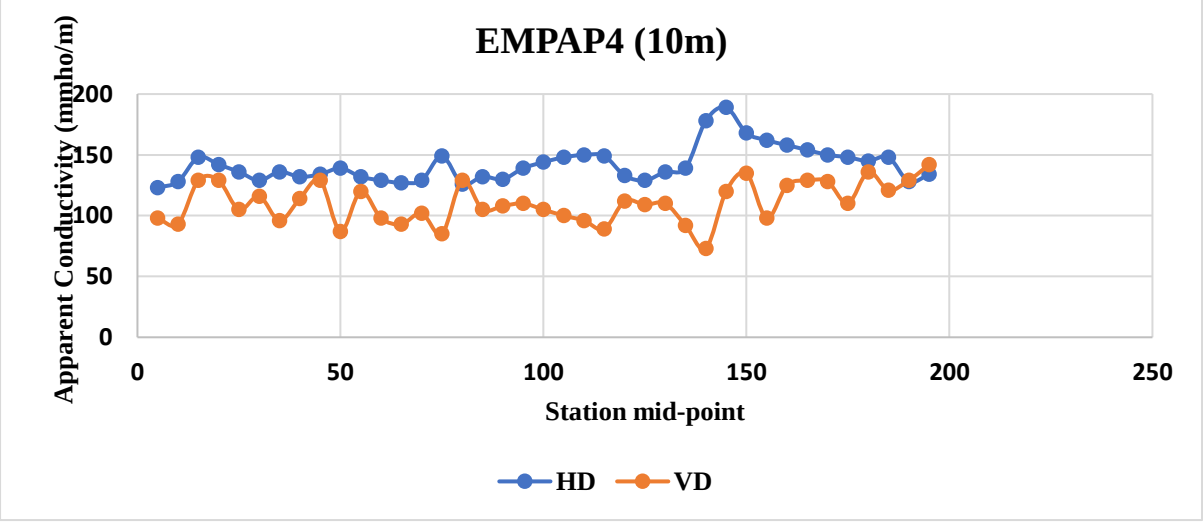

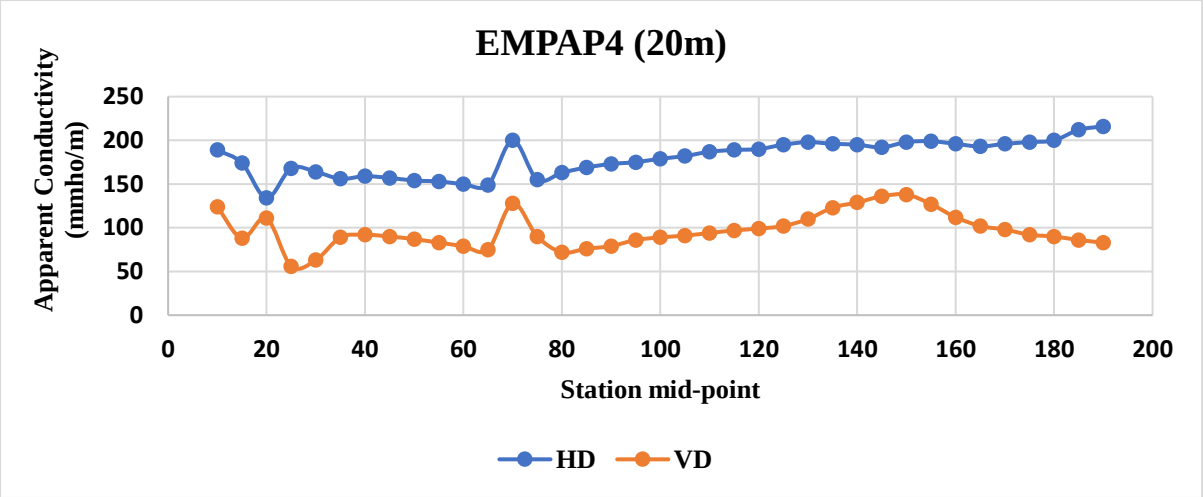

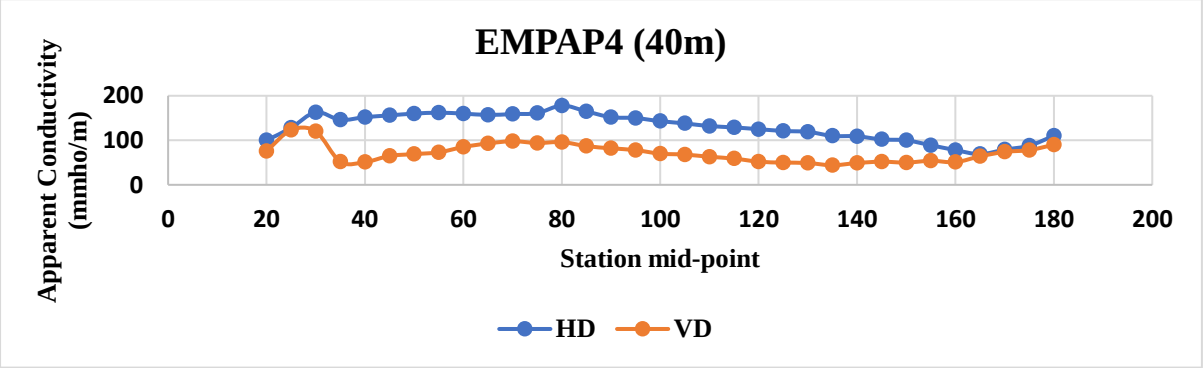

	True Conductivity (mS/m)		Depth (m)	
	HD	VD	HD	VD
1st Layer	150.59	86.29	7.8	11
2nd Layer	158.92	91.11	-	-

Figure 5d: Plot and Values of Apparent and Real Conductivity of Horizontal Dipole Orientations along Papalanto Traverse 2 (Profile 4)

Electromagnetic Profiling along Papalanto traverse 3 (EMT_3)

Fig. 5e and Fig. 5f shows the Apparent Conductivity Profiles (EMPAP5 and EMPAP6) along the third traverse EMT_3 conducted in the East and runs across the NW-SE direction of Papalanto study area at 10m, 20m and 40m seeking different investigation depths.

The traverse displays appreciable variation in conductivity except a distance of about 50 m to 150 m in Profile EMPAP5 and 20 m to 70 m in Profile EMPAP6 where there are few recognizable positive peaks and broad anomalies of about 159 mmho/m, 198 mmho/m, 143 mmho/m, 138 mmho/m, 201 mmho/m and 99 mmho/m which could be as a result of the weathering of the subsurface geological rock formations of the study area. These locations could be inferred as zones of interests in possible groundwater exploitation and consequently described as weathered to highly weathered/fractured zones which may serve as suitable aquifer for local and regional water supply of the study area (MacDonald *et al.*, 2005; (Ishola, 2019).). The observed varying degrees of conductivity values were delineated and presented in the plots with the most conductive area having a conductivity value of 201 mmho/m and the least conductive area having a conductivity value of 39 mmho/m respectively inferred to be conductive and resistive zones. Consequently, Vertical Electric Sounding of VESPAP11, VESPAPA12 and VESPAP13 were conducted in Profile EMPAP5 while VESPAP14 and VESPAP15 were conducted in Profile EMPAPAP6. On the contrary between the distance of between 150m to 200m in Profile EMPAP5 and 100m to 200m in Profile EMPAP6, the conductivity values at this point remain unchanged depicting the extension of the study locations to be relatively homogeneous and the study area not entirely fractured or weathered (Ugwu and Nwosu, 2009) consequently described as linear conductor (McNeil, 1980b) as displayed in the plots which presents a significant, extensive, uniform and linear distribution of

conductivities with less observable sinusoidal haphazard deviation thereby showing the results of the horizontal and vertical dipole orientations to be strongly correlative.

The high conductivity observed on both Profiles (EMPAP5 and EMPAP6) is indicative of probable invasions of the subsurface by the contaminant plumes. The high conductivity values (39 mmho/m-201 mmho/m in traverse 3) and (4 0mmho/m-205 mmho/m in traverse 4) within the lateral distance of about 50 m to 120 m by both the horizontal and vertical dipoles on both Profiles are suggestive that the subsurface is susceptible to invasions of contaminant seepages which may affect the underground regional water system of the investigated area.

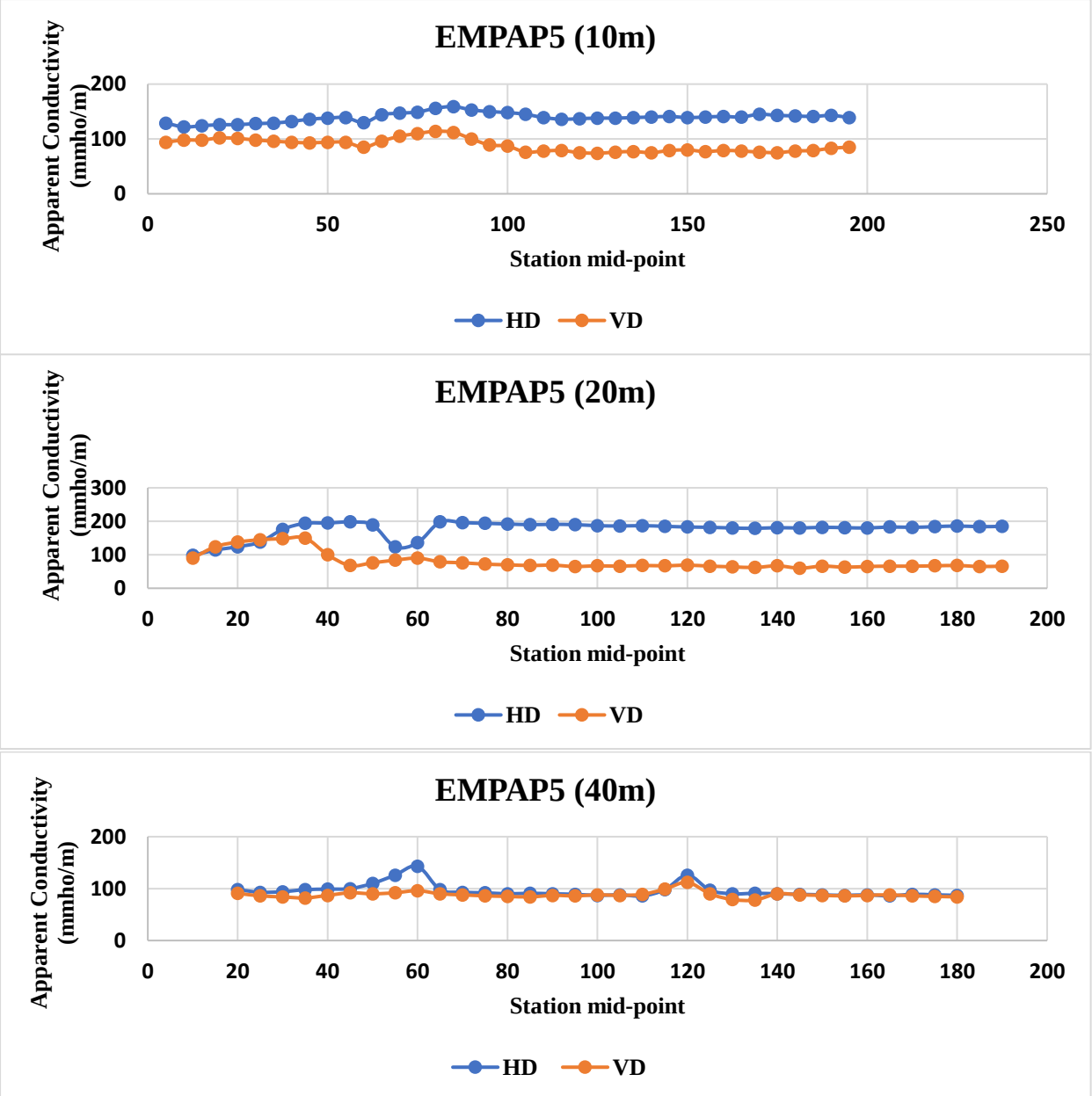

	True Conductivity (mS/m)		Depth(m)	
	HD	**VD**	**HD**	**VD**
1st Layer	131.15	87.32	8.9	16
2nd Layer	1141.92	94.55	-	-

Figure 5e: Plot and Values of Apparent and Real Conductivity of Horizontal Dipole Orientations along Papalanto Traverse 3 (Profile 5)

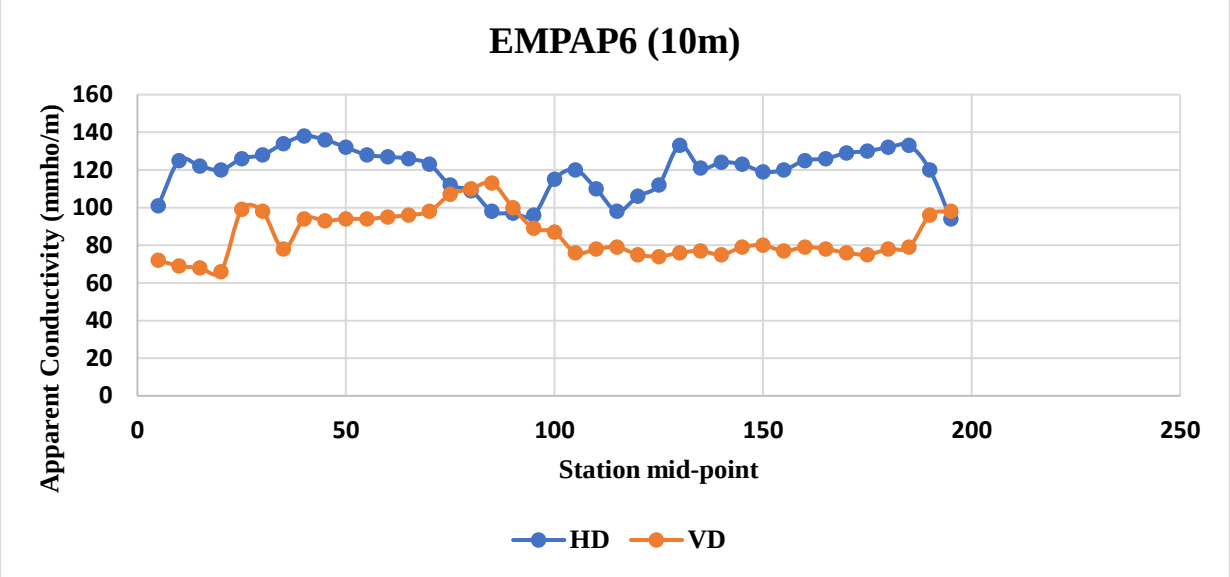

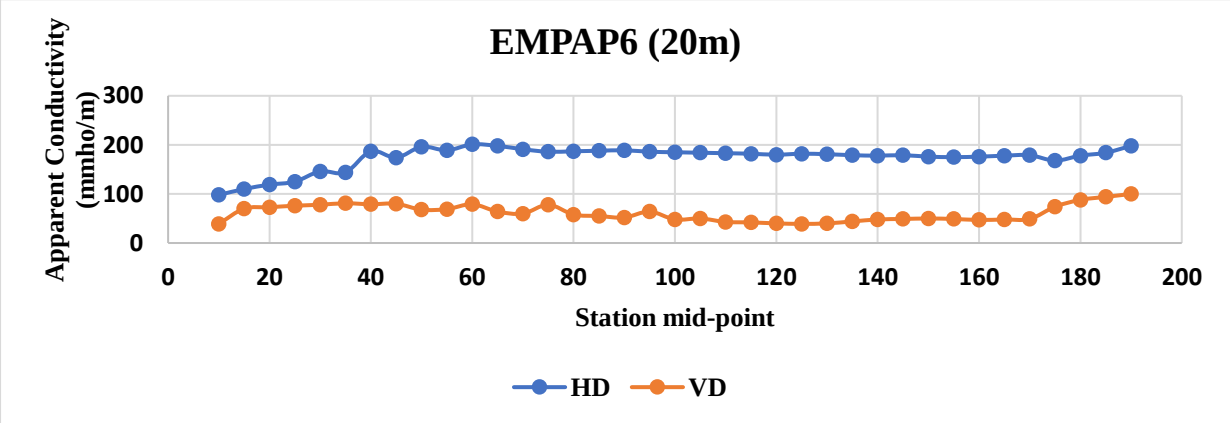

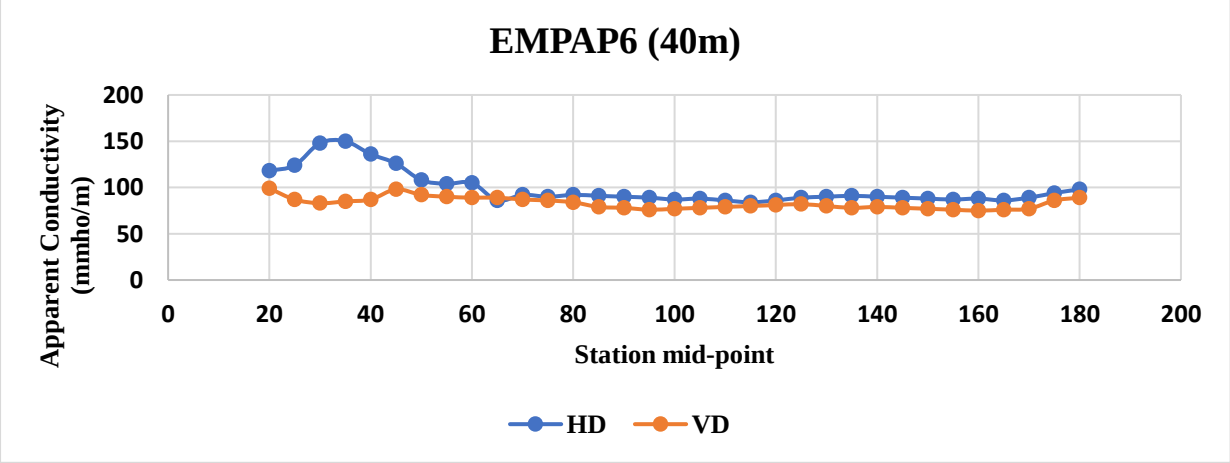

	True Conductivity (mS/m)		Depth(m)	
	HD	VD	HD	VD
1st Layer	138	78.9	2	17
2nd Layer	140.4	84.55	-	-

Figure 5f: Plot and Values of Apparent and Real Conductivity of Horizontal Dipole Orientations along Papalanto Traverse 3 (Profile 6)

Electromagnetic Profiling along Papalanto traverse 4 (EMT_4)

Fig. 5g and Fig. 5h shows the Apparent Conductivity Profiles (EMPAP7 and EMPAP8) along the fourth traverse EMT_4 conducted in the East and runs across the NW-SE direction of Papalanto study area at 10 m, 20 m and 40 m seeking different investigation depths.

The traverse displays significant variation in conductivity except a distance of about 10m to 50m and 50 m to 100 m in Profile EMPAP7 and 10 m to 70 m and 100 m to 200 m in Profile EMPAP8 where there are few observable positive peaks and broad anomalies of 205 mmho/m, 198 mmho/m, 179 mmho/m, 199 mmho/m, 172 mmho/m and 190 mmho/m.

The observed varying degrees of conductivity values were delineated as represented in the plots with the most conductive area having a conductivity value of 205 mmho/m and the least conductivity area having a conductivity value of 40mmho/m respectively inferred to be conductive and resistive zone. Consequently, Vertical and Electric Sounding of VESPAP16, VESPAP17 and VESPAP18 were conducted in Profile EMPAP7 while VESPAP19 and VESPAP20 were conducted in EMPAP8

Electromagnetic Profiling along Papalanto traverse 5 (EMT_5)

Fig. 5i and Fig 5j shows the Apparent Conductivity Profiles (EMPAP9 and EMPAP10) along the fifth traverse EMT_5 conducted in the East and runs across the NW-SE direction of Papalanto study area at 10 m, 20 m and 40 m seeking different investigation depths.

The traverse displays significant variation in conductivity except a distance of about 10m to 90m in Profile EMPAP9 and 50 m to 150 m in Profile EMPAP10 where there are few observable positive peaks and broad anomalies of about 198 mmho/m, 169 mmho/m, 137 mmho/m, 189 mmho/m, 222 mmho/m and 162 mmho/m which could be as a result of the weathering of the subsurface geologic structures in the study locations. The observed varying degrees of conductivity values were delineated as represented in the plots with the most conductive area having a conductivity value of 222 mmho/m and the least conductive area having a conductivity value of 45 mmho/m respectively inferred as conductive and resistive zones. Consequently Vertical Electric Sounding of VESPAP21 and VESPAP22 were conducted in Profile EMPAP9 while VESPAP23, VESPAP24 and VESPAP25 were conducted in Profile EMPAP10.

Varying high to very high conductivity value range 64 mmho/m to 198 mmho/m, 45 mmho/m to 169 mmho/m and 45 mmho/m to 137 mmho/m were respectively recorded for 10 m, 20 m and 40 m dipole spacing in a respective order obtained from the horizontal and vertical dipole orientations in the Electromagnetic Profiling of EMPAP9 while a conductivity range of values of 68 mmho/m to189 mmho/m, 55 mmho/m to 222 mmho/m, 52 mmho/m to 162 mmho/m were equally recorded in increasing order of 10 m, 20 m and 40 m dipole spacing observed on the horizontal and vertical dipole orientations on the Electromagnetic Profiling of EMPAP10 in a respective order of varying depth and resolution along the same traverse EMT_5.

The high conductivity observed on both Profiles (EMPAP9 and EMPAP10) is indicative of probable invasions of the subsurface by the contaminant plumes; this contaminant plume is related to leachates from the exotic materials and decaying wastes from the surface percolating the subsurface through the porous and permeable layers of overlying rock thereby migrating its ways down to the subsurface. The plots are presented in Fig. 5i and Fig. 5j while the distribution of Papalanto conductivity profiles the the corresponding layers for the investigated area are displayed in Fig. 6a to 7b.

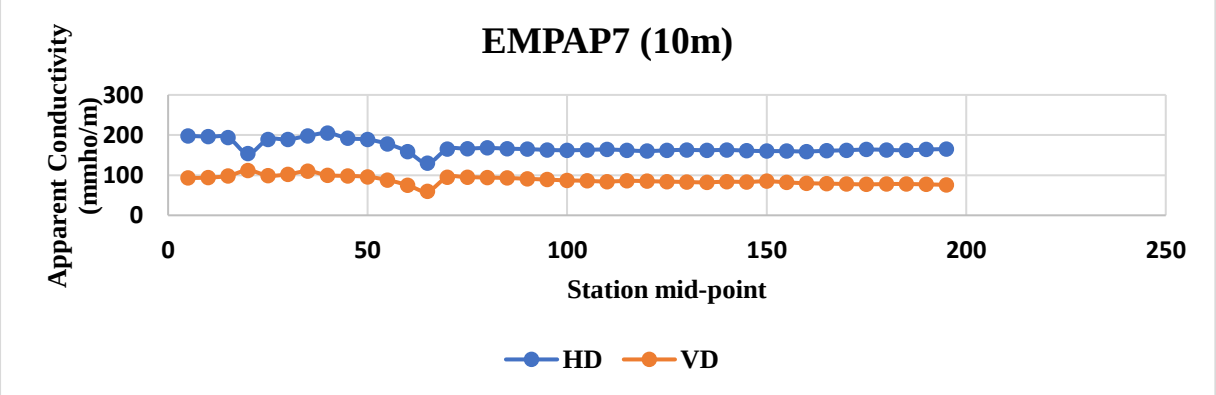

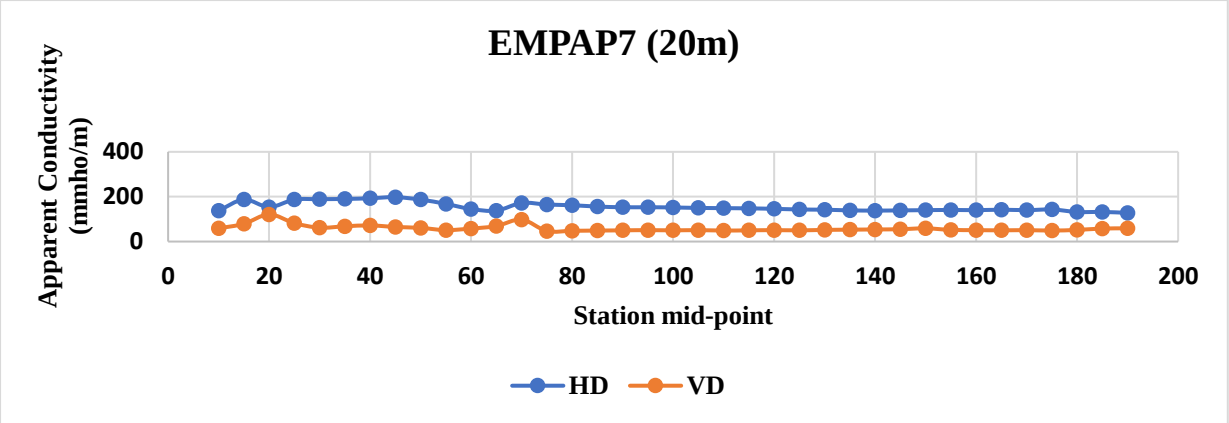

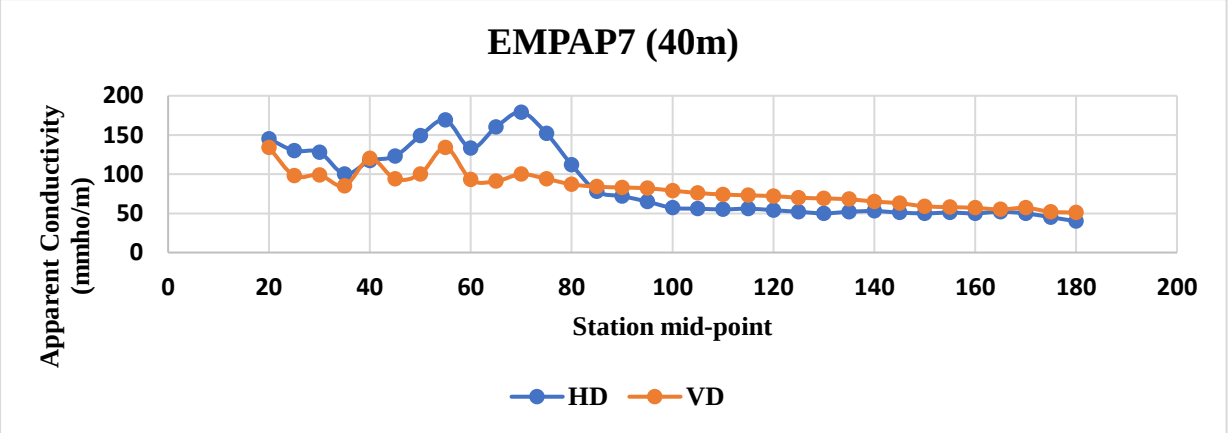

	True Conductivity (mS/m)		Depth(m)	
	HD	VD	HD	VD
1st Layer	167.48	96.78	7.8	9.2
2nd Layer	176.34	98.18	-	-

Figure 5g: Plot and Values of Apparent and Real Conductivity of Horizontal Dipole Orientations along Papalanto Traverse 4 (Profile 7)

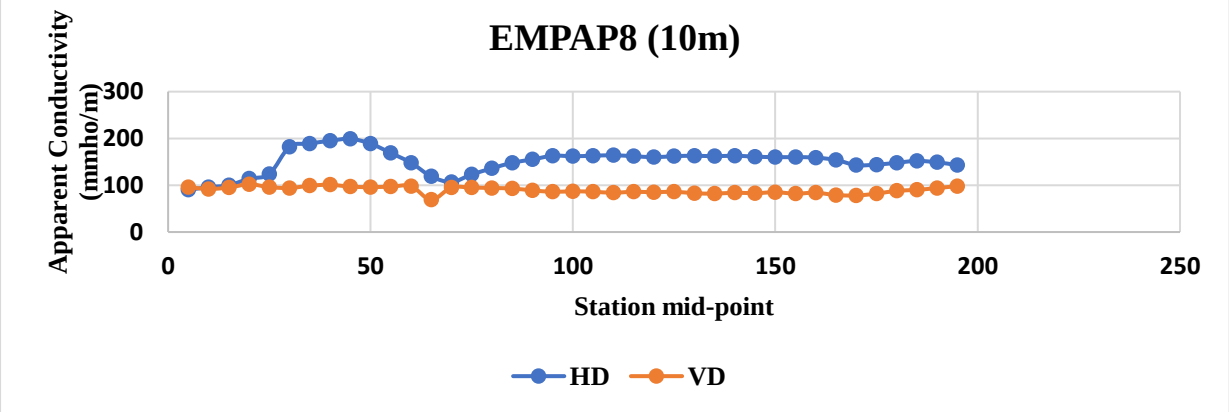

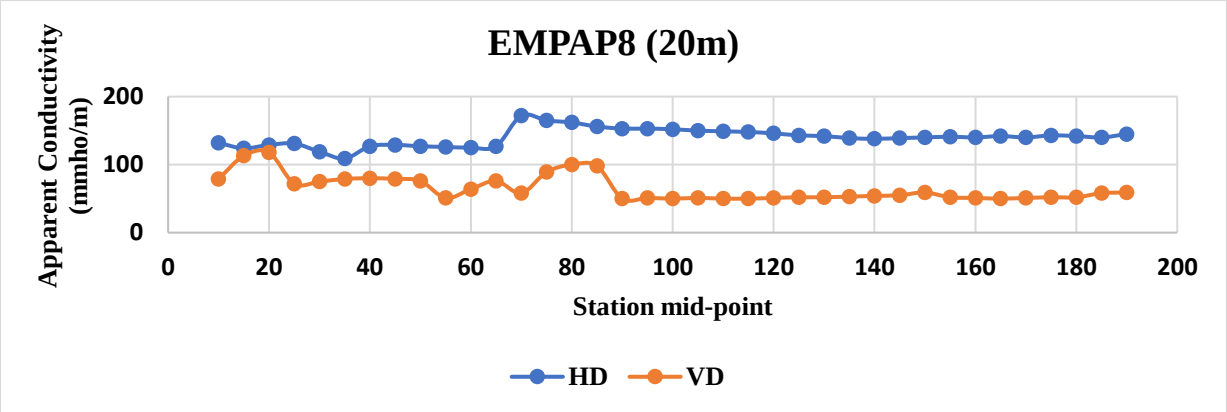

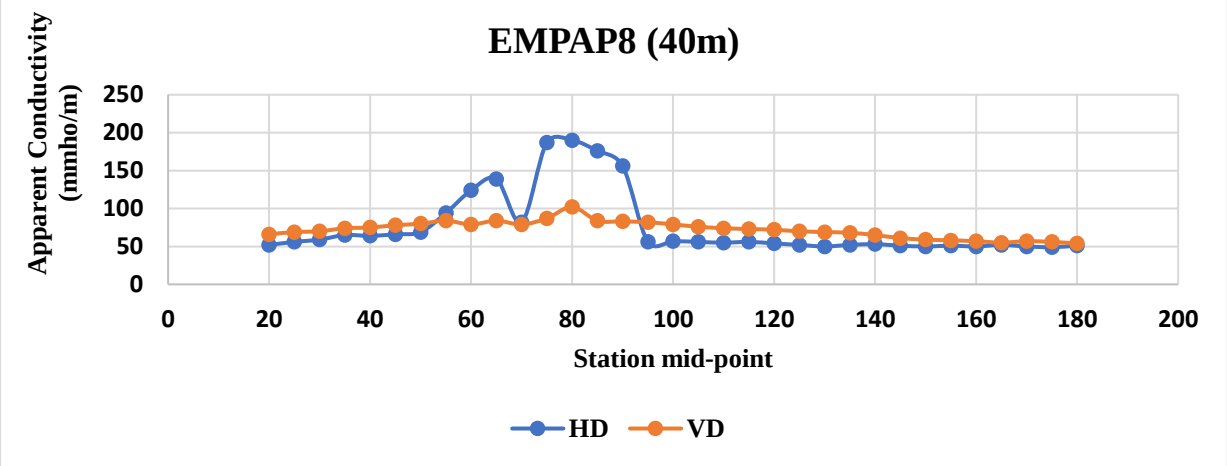

	True Conductivity (mS/m)		Depth(m)	
	HD	VD	HD	VD
1st Layer	143.32	98.6	8.4	6.5
2nd Layer	182.22	99.6	-	-

Figure 5h: Plot and Values of Apparent and Real Conductivity of Horizontal Dipole Orientations along Papalanto Traverse 4 (Profile 8)

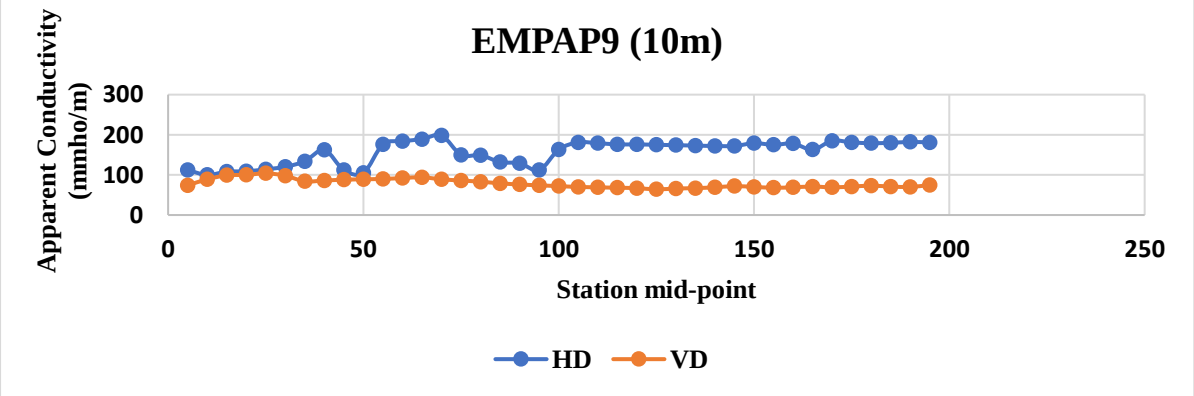

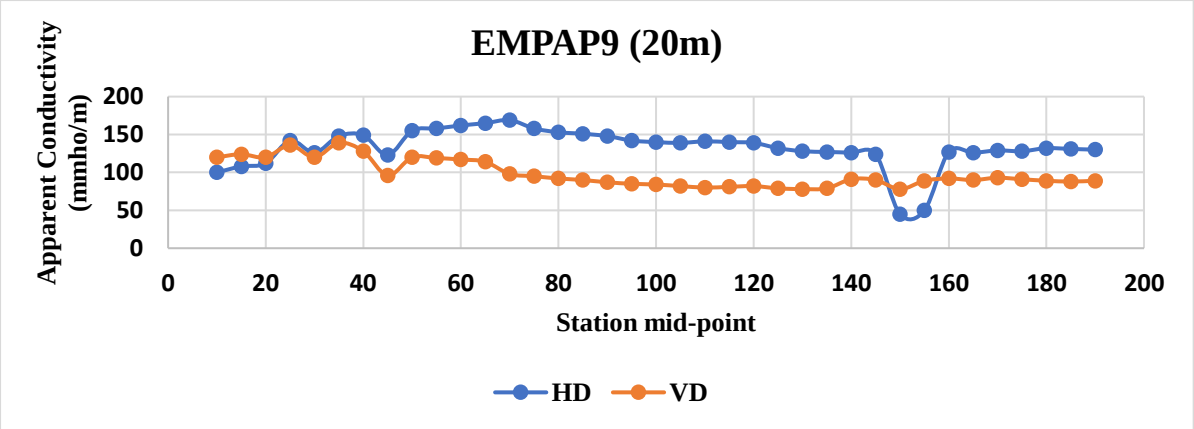

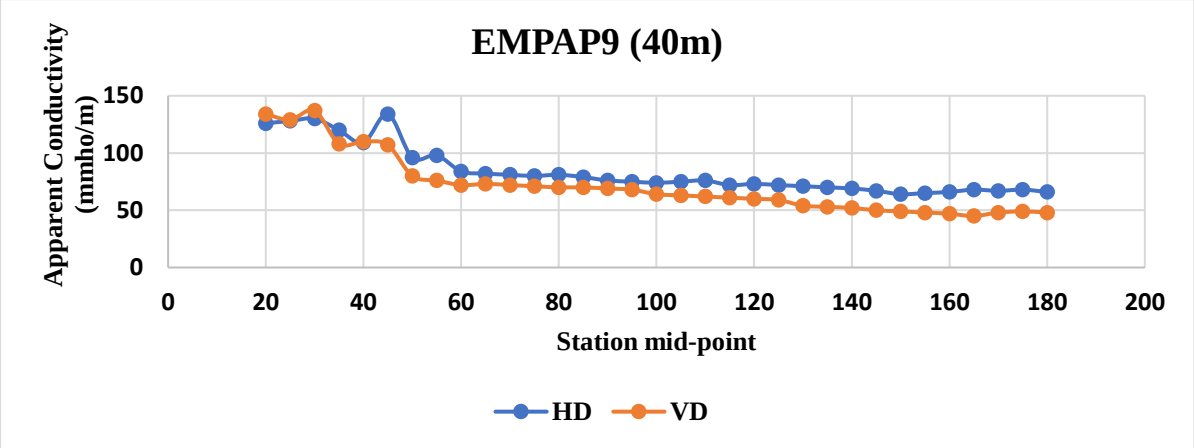

	True Conductivity (mS/m)		Depth(m)	
	HD	VD	HD	VD
1st Layer	121.13	106.92	3.1	10
2nd Layer	123.99	121.96	-	-

Figure 5i: Plot and Values of Apparent and Real Conductivity of Horizontal Dipole Orientations along Papalanto Traverse 5 (Profile 9)

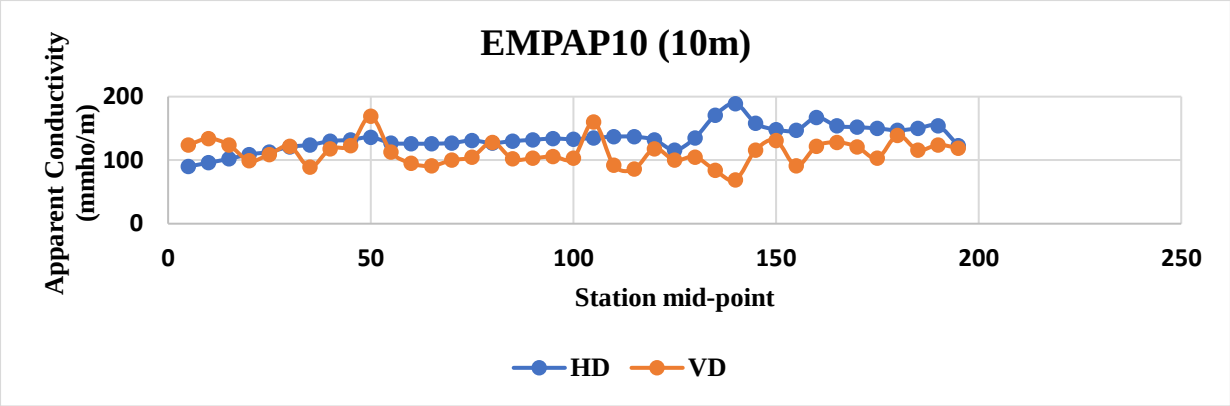

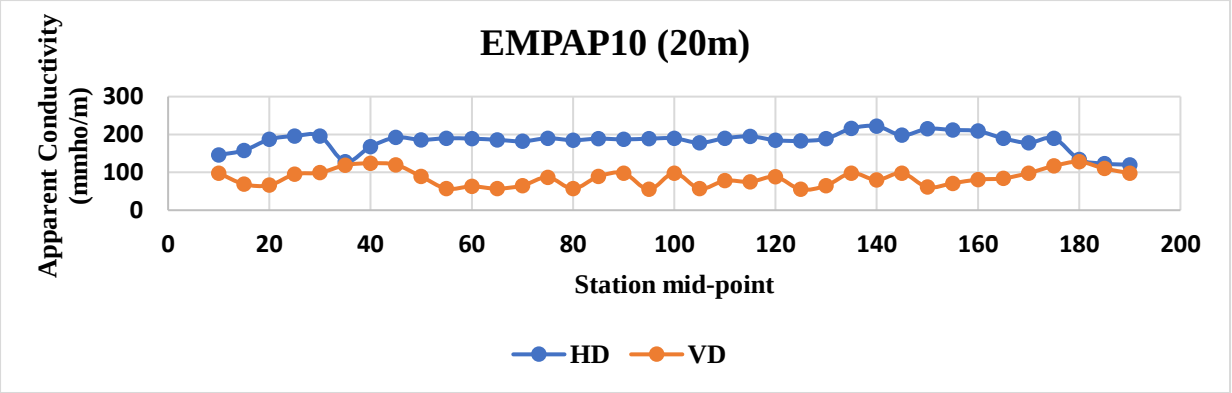

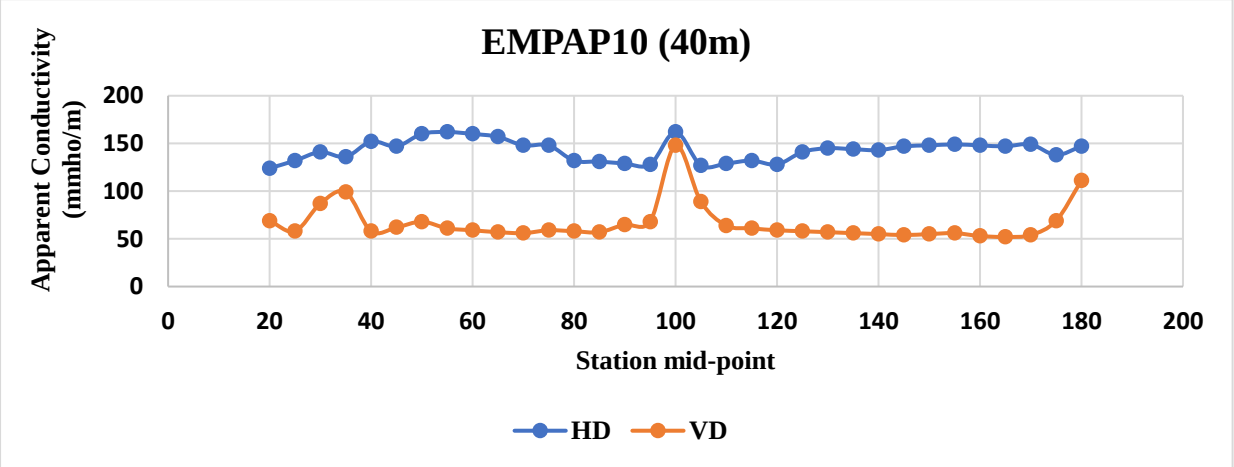

	True Conductivity (mS/m)		Depth(m)	
	HD	VD	HD	VD
1st Layer	130	115.88	33	10.4
2nd Layer	206	122.13	-	-

Figure 5j: Plot and Values of Apparent and Real Conductivity of Horizontal Dipole Orientations along Papalanto Traverse 5 (Profile 10)

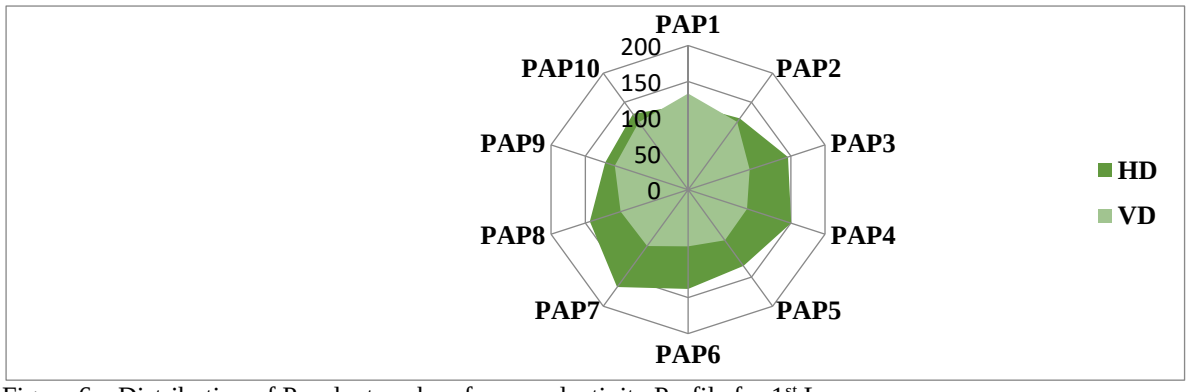

Figure 6a: Distribution of Papalanto subsurface conductivity Profile for 1st Layer

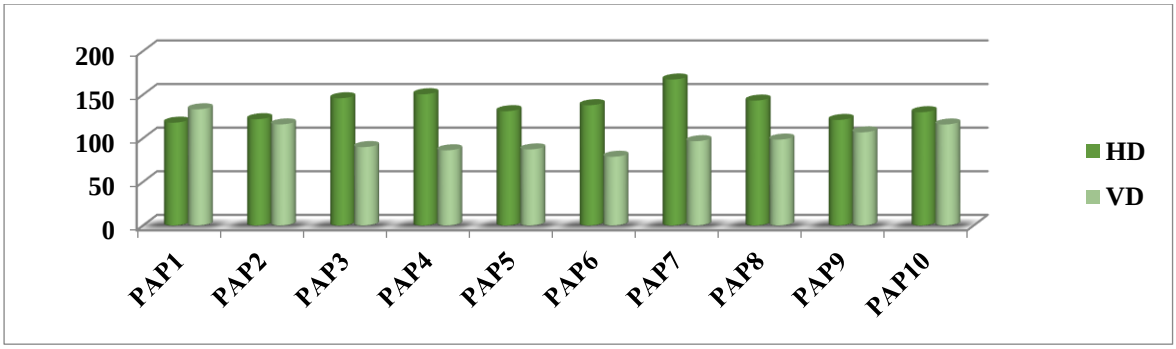

Figure 6b: Papalanto subsurface Conductivity Profile variation for 1st Layer

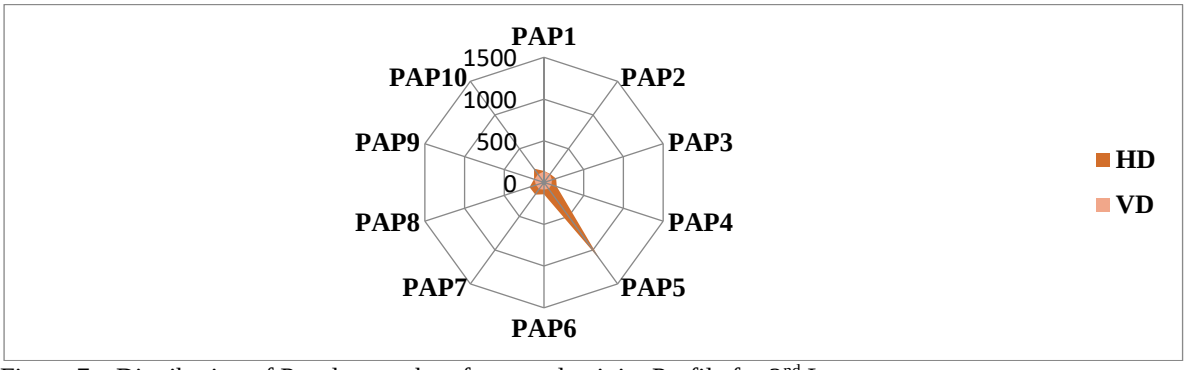

Figure 7a: Distribution of Papalanto subsurface conductivity Profile for 2nd Layer

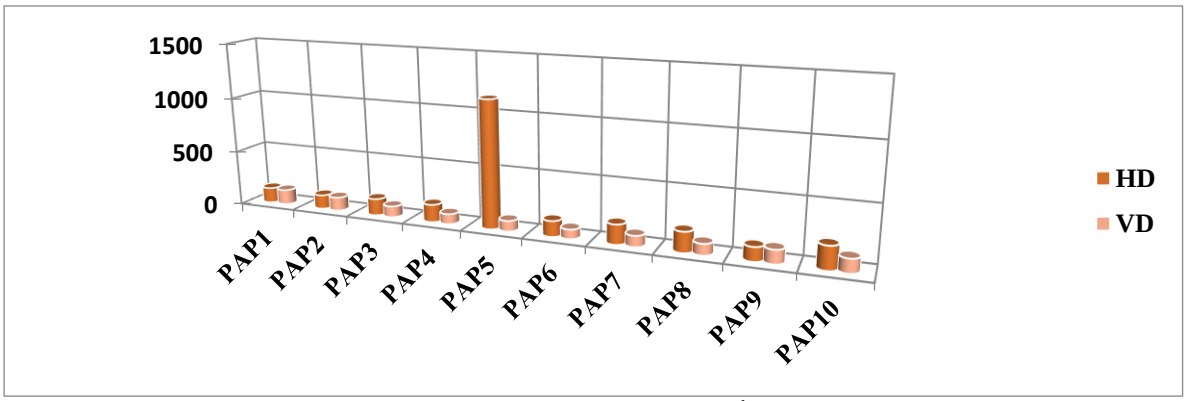

Figure 7b: Papalanto subsurface Conductivity Profile variation for 2nd Layer

Vertical Electrical Soundings

The results of the 25 VES soundings are presented as cross section through the subsurface in Fig. 8. Four principal geoelectric layers interpreted from the sounding stations include the Topsoil which is partly lateritic and alluvium, Sandy Clay/Clay/Silt, Sand/Clay/Shale, and Limestone/Sandstone. The resistivity values were calculated at different parts of the study area. The topsoil represents the uppermost geoelectric layer with resistivity of 9.78 Ω m to 1428Ω m. Thickness of the topsoil unit varies from 0.5–1.43 m. The topsoil is highly resistive in the north and north-east of the study. Geoelectric layers in this part of the study area include sand, shale, sand and clayey sand; these areas are devoid of leachate contamination. Four principal geoelectric layers inferred from the VES data include the Topsoil is partly lateritic and alluvium, Sandy Clay/Clay/Silt, Sand/Clay/Shale, and Limestone/Sandstone. Resistivity values for these layers vary from 9.78 Ωm to 1428 m, 1.46 Ωm to 1057 Ωm, 1.46 Ωm to 451 Ωm, and 15 Ωm to 10,000 Ωm with corresponding thickness of 0.5–1.43, 1.29–13, 2.8–84.4 m and infinity, respectively. The second geoelectric layer is Sandy Clay/Clay sometimes Silt characterized as, contaminated. This layer has resistivity and thickness of 1.46 to 1057 Ωm, and 1.29–13m, respectively. At VESPAP24, the dry sands have resistivity of 1057 Ω m with thickness of 1.7 m. The

general low resistivity value is attributed to leachate infiltration. Sandy clays are the dominant type of rock type in the study area. They are interpreted at all the VES stations. The sands are presumably composed of sand with relatively low resistivity and coarse and fine alluvium sands with higher resistivity value .The saturated unit represents the aquiferous zone in the study area with thickness of 1.46 m to 451 m. At shallow depth, the sands are interpreted as the vadose zones and as multi-aquiferous layers at deeper stratigraphic levels. The depth to the vadose zone unit ranges from 2.72 m to 96.5 m. Underneath the sand are Clayey Sands, Limestone and Sandstone with relatively higher resistivity values as compared to the overlying sands. The fourth geoelectric layer is limestone underlain by Sandstone with intercalations of clayey or shaly horizon with resistivity values of 15 to 10,000 Ωm with corresponding maximum depth of 87.7 m and infinity, the actual thickness of this layer could not be estimated as they represent the last units on the lithology logs. However, they are estimated at depths of > 60 m at these VES stations.

VESPAP1 **VESPAP2** **VESPAP3** **VESPAP4**

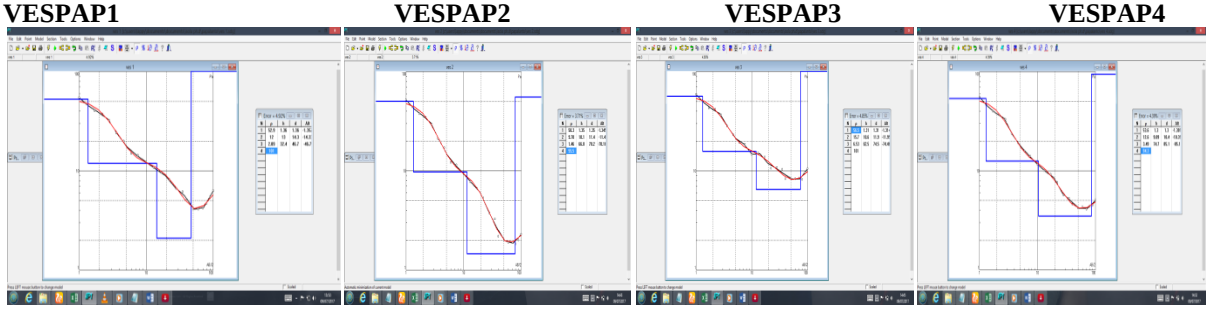

VESPAP5 **VESPAP6** **VESPAP7** **VESPAP8**

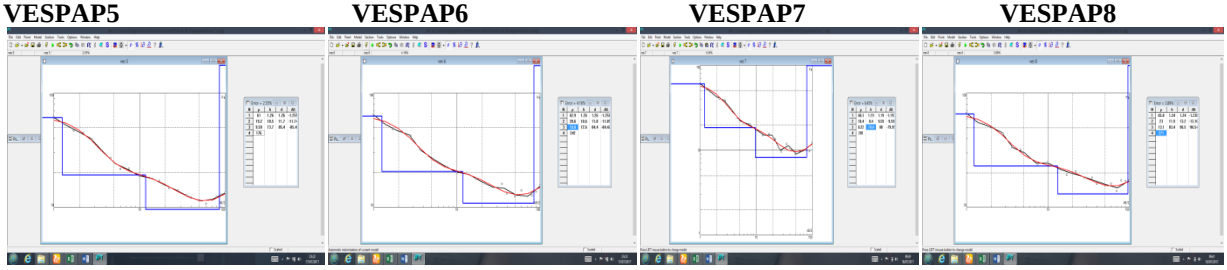

VESPAP9 **VESPAP10** **VESPAP11** **VESPAP12**

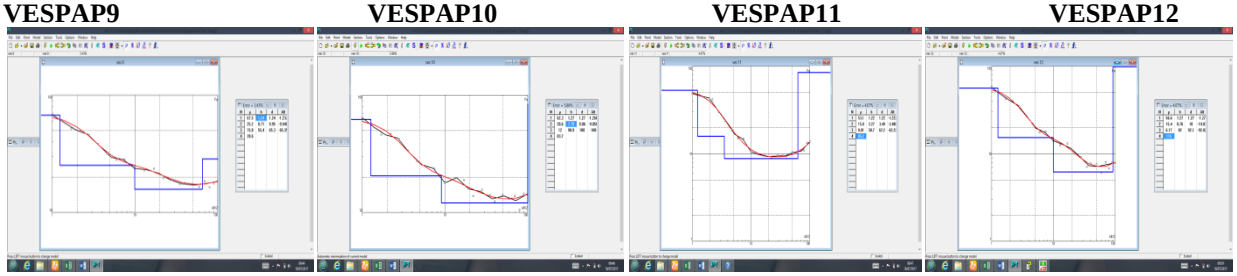

VESPAP13 **VESPAP14** **VESPAP15** **VESPAP16**

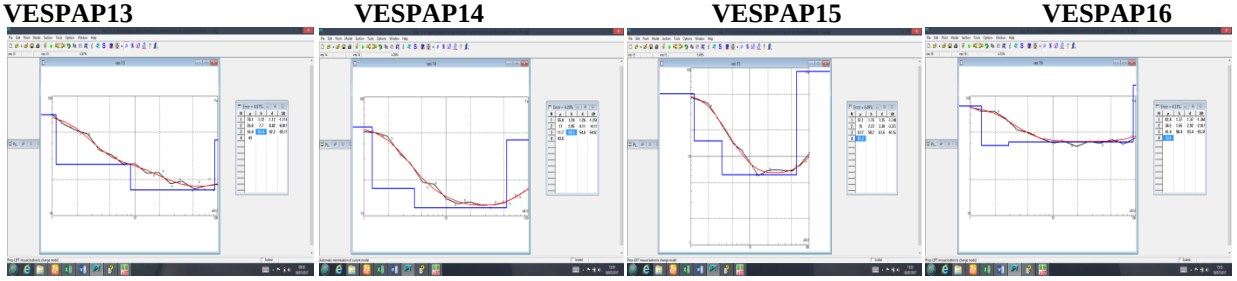

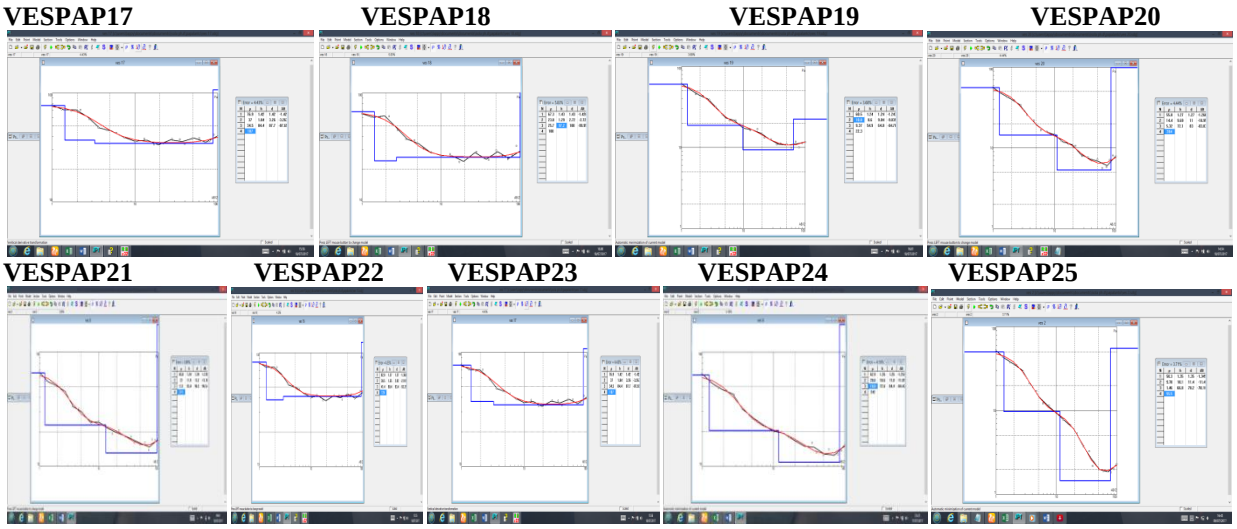

Figure 8: Cross section through VESPAP1 to VESPAP25

Aquifer Vulnerability and Overburden Protective Capacity

The inferred degree or state of leachate contamination with respect to the values of the estimated longitudinal conductance (S*i*) range from 0.0007264 mho to 0.668 mho in the study area (Table. 2). The highest value of S*i* was obtained at stations VESPAP2 followed by VESPAP13 and VESPAP19 while VESPAP22 exhibited the lowest conductance. When correlated with the values of overburden protective capacity of Table 4.2. It shows that aquifers in the study area have poor protective capacity and are thus vulnerable to leachate pollution when compared to the standard of Oladapo *et al.*, 2004 and Van Stempvoort *et al.*,1992 (Table. 1).

Table 1: Rating and Classification of Aquifer Vulnerability on the Basis of Protective Capacity using values of Longitudinal Conductance and Hydraulic Resistance

S*i* (mho)	**Protective Capacity rating**	**Log c (hydraulic resistance)**	**Vulnerability Implication**
	(Oladapo *et al.*, 2004)		**(Van Stempvoort *et al.*, 1992)**
>10	Excellent	>4	Very Low to Extremely Low Vulnerability
5–10	Very good	3–4	Low Vulnerability
0.7–4.9	Good	2–3	Moderate Vulnerability
0.2−0.69	Moderate	1–2	High Vulnerability
<0.1−0.9	Poor–weak	<0.5−1	Very High to Extremely High Vulnerability

Table. 2: Vertical Travel Time Estimate of Vadose Zone Material in Papalanto

Lithology	**Thickness**	**K(cm/s)**	$C_i = \sum_{i=1}^{N} \frac{d_i}{K_i}$	**C(second)**	**C(hour)**	**C(day)**	**Log C**	**Hydrogeological Vulnerability Implication**
	1.36	3.545958	3836.000184					
VESPAP1	13	4.9346826	26344.14623	91316.28456	25.3656	1.0569	0.0240	VHV
	32.4	5.2996478	61136.13814					
	1.35	5.71435245	2650.473728					
VESPAP2	10.2	5.01419245	20342.2589	148168.3937	41.1579	1.7149	0.2342	VHV
	66.8	5.32237416	125475.6617					
	1.31	3.581882	3657.295243					
VESPAP3	10.6	4.8049583	22060.54525	147481.366	40.9671	1.7070	0.2322	VHV
	62.5	5.132908	121763.5255					
	1.3	3.657458	3554.381212					

Lithology	Thickness	K(cm/s)	$C_i = \sum_{i=1}^{N} \frac{d_i}{K_i}$	C(second)	C(hour)	C(day)	Log C	Hydrogeological Vulnerability Implication
VESPAP4	9.09	4.9134108	18500.38674	36292.84309	10.0814	**0.4201**	**-0.3767**	**EHV**
	74.7	5.2464957	14238.07514					
	1.26	3.4676889	3445.015637					
VESPAP5	10.5	4.6853863	22410.10522	172636.9784	47.9547	1.9981	0.3006	VHV
	73.7	5.0210565	146781.8576					
	1.26	3.420574	3683.592286					
VESPAP6	10.6	4.6383948	22852.73345	172392.5914	47.8868	1.9953	0.3000	VHV
	72.6	4.977503	145856.2657					
	1.19	3.4852102	3414.428203					
VESPAP7	8.4	4.712452	17825.11525	160072.8503	44.4647	1.8527	0.2678	VHV
	70.4	5.0708293	138833.3068					
	1.24	3.3498928	3701.610989					
VESPAP8	11.9	4.5589319	26102.60531	200155.9025	55.5989	2.3166	0.3649	VHV
	83.4	4.8957543	170351.6862					
	1.24	3.3091401	3747.197044					
VESPAP9	8.71	4.4872873	19410.39077	138538.198	38.4828	1.6035	0.2051	VHV
	55.4	4.48015	115380.6102					
	1.27	3.4304394	3702.149643					
VESPAP10	7.79	4.6417357	16782.51521	57631.19744	16.0087	0.6670	-0.1759	EHV
	28.2	4.9344683	57146.53259					
	1.22	3.6706485	16945.23461					
VESPAP11	2.27	4.8015	4727.689264	137925.8769	38.3127	1.5964	0.2031	VHV
	58.7	5.0049334	116252.953					
	1.27	3.579304	3872.773003					
VESPAP12	8.76	4.8153482	18191.82086	126607.1465	35.1687	1.4654	0.1659	VHV
	53.8	5.11462298	104542.5527					
	1.12	3.2477692	3448.520911					
VESPAP13	7.7	4.4358904	17358.40904	130621.1364	36.2837	1.5118	0.1794	VHV
	52.5	4.7808022	109814.2065					
	1.26	3.5999803	3500.019153					
VESPAP14	2.85	4.7601937	5987.151321	111603.2358	31.0009	1.2917	0.1112	VHV
	50.5	4.9453531	102116.0653					
	1.15	3.7239883	3300.969466					
VESPAP15	2.23	4.828292	4617.707263	121143.1264	33.6508	1.4021	0.1468	VHV
	58.2	5.1402298	113224.5120					
	1.37	2.9639664	4622.184651					
VESPAP16	1.55	4.0775176	3801.332458	192734.0019	53.5372	2.2307	0.3485	VHV
	73.6	3.9933262	184310.4848					
	1.42	3.025882	3555.990332					
VESPAP17	1.84	4.1217934	4464.077327	209422.3141	58.1729	**2.4239**	**0.3845**	**VHV**
	84.4	4.1906186	201402.2464					
	1.43	3.3139087	4315.146039					
VESPAP18	1.29	4.5327479	2845.955761	140638.7049	39.0663	1.6278	0.2116	VHV
	59.68	4.4711621	133477.6031					
	1.24	3.4801951	3563.018637					

Lithology	Thickness	K(cm/s)	$C_i = \sum_{i=1}^{N} \frac{d_i}{K_i}$	C(second)	C(hour)	C(day)	Log C	Hydrogeological Vulnerability Implication
VESPAP19	8.60	4.6988996	1830215738	131031.6589	36.3977	1.5166	0.1809	VHV
	54.9	5.0290161	109166.4829					
	1.27	3.5999803	2267.865121					
VESPAP20	9.69	4.8501438	19978.78908	161494.4108	44.8596	1.8692	0.2716	VHV
	72.1	5.1778213	139247.7566					
	0.5	2.1873447	2285.876574					
VESPAP21	0.72	4.8292364	1490.918937	85327.76869	23.7022	0.9876	-0.0054	EHV
	4.85	4.8292364	10042.99562					
	32.6	4.5589319	71507.97756					
	0.9	0.00018431	48831760.17					
VESPAP22	2.95	0.93527785	31541.42903	48864274.84	27462.30	1144.26	3.0586	MV
	1.9	48.292364	393.4369417					
	2.8	48.292364	579.8018088					
	1.6	4.1515774	3853.956812					
VESPAP23	45.72	5.0062562	11425.70374	96217.34398	26.7270	1.1136	0.04674	EHV
	5.32	3.3210744	16018.91243					
	32.5	5.0062562	64918.77104					
	1.1	0.92856804	11846.19713					
VESPAP24	1.7	0.002664457	6380010.168	6512240.34	1808.9557	75.3732	1.8772	HV
	1.63	0.209190151	77919.53827					
	8.96	2.1100009	42464.43686					
	1.4	0.007407135	1890069.643					
VESPAP25	1.94	1.8402259	10542.18398	1954133.146	54281.48	22.6173	1.3544	HV
	3.25	4.5589319	7128.862793					
	13.83	2.9810881	46392.45654					

The AVI method indicates the rate of hydraulic resistance to vertical flow and pollution introduced from the surface as shown in Table 1. Log c is <0.5–1 (Very High to Extremely High Vulnerability), log c = 1–2 (High Vulnerability), Log c = 2–3 (Moderate Vulnerability) and Log c = 3–4 (Low Vulnerability) and Log c >4 (Very Low to Extremely Low Vulnerability). The AVI method categorised major areas of the study area as a high to extremely high vulnerability zone with less than 10% categorised as having moderate vulnerability. AVI index parameters are solely based on the layer thickness and its hydraulic conductivity. Aquifer vulnerability index in the study area has revealed that the degree of contamination decreases with depth along the investigated profile locations Aquifers in the study area are not naturally protected by any lithological barrier to leachate seepage.

Clayey geoelectric layers in the study area are located farther from the aquifer zone and are mixed variably with coarse and fine grained alluvium sands thereby making the soil and aquifers of the study area to be vulnerable to leachate contamination at shallow levels. Since we interpreted the topsoil as being lateritic soils and alluvium in very few places with less clayey content, leachate infiltration in the study area is enhanced by the lack of protective layers as shown by the correlation between longitudinal conductance and overburden protective capacity. The topsoil in the the study area is porous and permeable and is therefore conduits for leachate. Hence, the soils and groundwater resources around the investigated locations of the study area might be polluted by possible contaminant seepages from different environmental sources. This necessitates the use of direct geochemical analyses to prove the toxicity of the existing groundwater of the area in form of boreholes and hand-dug wells. We hypothesize that with time the leachate contamination may contribute to pollution of the groundwater and this is of great threat to domestic usage, farming and future exploitation of underground water resources in the study area.

CONCLUSION

The varying calculated true conductivity values were consequently recorded with the corresponding depth values in all the investigated profiles in the study area both for the horizontal and vertical dipole orientations for the first layer and the second layer. 1141.92

mmho/m was recorded as the highest true conductivity value for the Horizontal Dipole in the second layer; this occurred in Profile EMPAP5 while the highest true conductivity value for the Vertical Dipole in the first layer was 134.31 mmho/m which occurred in Profile EMPAP1. The appreciable variation in conductivity with recognizable positive peaks and broad bowl shaped anomalies observed in the study area which could be as a result of weathering of the subsurface geological horizon in the study locations and the observed high conductivity values in both the horizontal and vertical dipole orientations are indicative of the vulnerability of its subsurface hydrogeological environment to invasion of contaminant seepages and consequent possible pollution of the investigated locations of the study area. The results of the Electrical resistivity methods revealed that the topsoil is characterized at shallow depth by zone of abnormally low resistivity values suggestive of the presence of a highly conductive fluid or rock type. This observation was made along the profile lines and on the VES stations. Hence, we interpret the anomalous zone as areas of leachate contamination. Leachate plumes normally have low resistivity values because of high ion concentration (Rosqvist et al., 2003). In this work, the leachate plume have resistivity of 0.2 –10 Ω m while for electrical sounding, the resistivity of the leachate is 3.38 – 67 Ω m. The resistivity of the leachate plume in this work is in accordance with the result obtained by previous workers such as Hamzah et al., 2014 as 1–10 Ω m and Ariyo et al., 2013 as <6 Ω m. Consequently, the low resistivity values could have been attributed to clayey rock in the topsoil. However, the topsoil in the study area is generally lateritic and partly alluvium and composed of coarse and fine sands. An important observation is that the lowest resistivity values were estimated around the dumpsites when compared to the rest of the study area. An important aspect of leachate contamination is the generation and migration. Previous authors favoured infiltrated rainfall as the principal source of leachate generation. In the study area, secondary sources may include effluents such as liquid waste and slurries which may account for the restricted spread of the leachate to the dumpsite and surrounding residential area. Aquifer vulnerability index in the study area shows that the degree of contamination decreases with depth along the investigated profiles and that soil and aquifers of the study area are vulnerable to leachate contamination at shallow levels. Since we interpreted the topsoil as being lateritic soils with less clayey content, leachate infiltration in the study area is enhanced by the lack of overburden protective layers as shown by the correlation between longitudinal conductance and overburden protective capacity. The topsoil in the southwestern part of the study area is porous and permeable and is therefore conduits for leachate. Hence, the soils and groundwater resources around the study area might be polluted by the leachate. Although, there is no direct geochemical analysis to prove that the soils and groundwater are toxic. We hypothesize that with time the leachate contamination may contribute to pollution of the groundwater and this is of great threat to farming and future exploitation of underground water resources in the area. This work shows that study area is highly susceptible to pollution by the gradual invasions of the leachate contaminant seepages. To forestall further pollution of the soil and groundwater aquifers in the study area, we recommend planned and engineered landfill and also enlightenment campaign to stop indiscriminate dumping practices. The government has huge responsibility of ensuring compliance with existing landfill laws and the provision of suitable dumpsite for the residential area whose population, domestic and industrial activities are on daily increase.

REFERENCES

Adewumi I.K, Ogedengbe M.O, Adepetu J.A, Fabiyi Y.L. 2005. Planning organic fertilizer industries for municipal solid wastes management. J Appl Sci Res 1(3):285–291Google Scholar

Akinmosin A.A, Omosanya K.O, Ige T. 2013. The occurrence of Bitumen in Ijebu-itele, Eastern Dahomey Basin, SW, Nigeria. ARPN J Sci Technol 3(1):98–105Google Scholar

Agagu, O.K. 1985. A Geological Guide to Bituminous Sediments in Southwestern Nigeria. Dept. Geol. Univ. Ibadan, pp. 212.

Ariyo, S.O., and Adeyemi, G. O. 2009. Role of Electrical Resistivity Method for Groundwater

Ariyo S.O, Omosanya K.O, Oshinloye B.A (2013). Electrical resistivity imaging of contaminant zone at Sotubo dumpsite along Sagamu-Ikorodu Road, Southwestern Nigeria. Afr J Environ Sci Technol 7:312–320Google Scholar

Bayode S, Omosuyi G.O, Mogaji K.A, Adebayo S.T. 2011. Geoelectric delineation of structurally-controlled leachate plume around Otutubiosun dumpsite, Akure, Southwestern Nigeria. J Emerging Trends Eng Appl Sci 2(6):987–992Google Scholar

Billman H.G. 1992. Offshore stratigraphy and paleontology of the Dahomey Embayment, West African. Niger Assoc Pet Explor Bull 7(2):121–130Google Scholar

Burschil T, Scheer W, Kirsch R, Wiederhold H. 2012. Compiling geophysical and geological information into

a 3-D model of the glacially-affected island of Föhr. Hydrol Earth Syst Sci 16:3485–3498CrossRefGoogle Scholar

Coker S.L and Ejedawe J.E 1983. Hydrocarbon source potential of Cretaceous Rock of Okitipupa uplift; Nigeria Journal of Mining and Geology; Vol. 20pp 168-169.

Desa N.D, Mejus L, Abd Rahman M, Samuding K, Mostapa R, Dominic J.A. 2009. Study on subsurface contamination flow path distribution using Electrical Resistivity Imaging (ERI) technique at waste disposal site, Taiping, Malaysia. In: Proceedings of SEG Houston 2009 international exposition and annual meetingGoogle Scholar

Faneca Sànchez M, Gunnink J.L, Van Baaren E.S, Oude Essink G.H.P, Siemon B, Auken E, Elderhorst W, De Louw P.G.B. 2012. Modelling climate change effects on a Dutch coastal groundwater system using airborne electromagnetic measurements. Hydrol Earth Syst Sci 16:4499–4516. doi:10.5194/Hess-16-4499-2012 CrossRefGoogle Scholar

Fidelis U., Thomas H. and Uduak A. 2014. Reserve Estimation from Geoelectrical Sounding of the Ewekoro Limestone at Papalanto, Ogun State, Nigeria.Journal of Energy Technologies and Policy. ISSN 2225-0573, www.iiste.org Vol.4, No.5, 2014, pp 28-33

Freeze R.A, and Cherry J.A. 1979. Groundwater. Prentice Hall, New Jersey Google Scholar

Gbadegesin, S.A. 1992. Soils In: Ogun State in Maps, Onokomaya, K. Oyesiku and J. Jegede (Eds) Rex Charles Publication, Nigerian Paper Pp 207

.

Hamzah U, Mark J, Nur Atikah M.A. 2014. Electrical resistivity techniques and chemical analysis in the study of leachate migration at Sungai Sedu Landfill. Asian J Appl Sci 7:518–535CrossRef Google Scholar

Henriet JP. 1976. Direct application of the Dar Zarrouk parameters in groundwater surveys. Geophys Prospect 24:344–353CrossRef Google Scholar

Herbst, M, Hardelauf, H, Harms, R, Vanderborght, J and Vereecken, H. 2005. Pesticide fate at regional scale: Development of an integrated model approach and application, Physics and Chemistry of the Earth 30(8–10), pp. 542–549.

Herckenrath D, Fiandaca G, Auken E, Bauer-Gottwein P. 2013. Sequential and joint hydrogeophysical inversion using a field-scale groundwater model with ERT and TDEM data. Hydrol Earth Syst Sci 17:4043–4060CrossRefGoogle Scholar

Idornigie A.I, Olorunfemi M.O, Omitogun A.A 2006. Electrical resistivity determination of surface layers, soil competence and soil corrosivity at an engineering site location in Akungba-Akoko, Southwestern Nigeria. Ife J Sci 8(2):159–177Google Scholar

Jones H.A, Hockey R.D. 1964. The geology of part of Southwestern Nigeria. Geol Survey Niger Bull 31:87Google Scholar

Keary, P., and Brooks M. 1991. An Introduction to Geophysical Exploration (2nd Edition). Oxford, Blackwell, .Blackwell Scientific Publications, London. pp. 254.

Kehinde-Phillips, T. Ogun State maps, In: Onakomaya, S.O., K. Oyesiku and Jegede. 1992. Ogun State in Maps. Rex Charles Publishers, Ibadan, pp: 187, Ibadan, pp187, 1992.

Kirsch R. 2006. Groundwater protection: vulnerability of aquifers. In: Kirsh R (ed) Groundwater geophysics a tool for hydrogeology. Springer, Berlin, Heidelberg, pp 468–480Google Scholar

Lasserre, F, Razack, M and Banton, O. 1999. A GIS-linked model for the assessment of Nitrate Contamination in Groundwater, J. Hydrol. 224(3–4), pp. 81–90.

Mamah L. I. and Eze, L. C. 1988. Electromagnetic and ground Magnetic Survey over Zones of Lead-Zinc Mineralization in Wanakom (Cross River State). Journal of African Earth Sciences, Vol. 7, No.5-6, pp. 749-758.

McLay, C. D.A, Dragden, R, Sparling, G and Selvarajah, N. 2001. Predicting Groundwater Nitrate Concentrations in a Region of Mixed Agricultural Land Use a Comparison of Three Approaches, Environmental Pollution, vol. 115, pp.191–204

McNeill, J. D. 1980b. EM 34-3 Survey interpretation techniques. Technical note: TN-8. Geonics Ontario. pp. 1-17.

Nton, M.E. 2001. Sedimentological and geochemical studies of rock units in the eastern Dahomey Basin, southwestern Nigeria, unpublished Ph.D thesis, University of Ibadan, pp. 315.

Oladapo M.I, Mohammed M.Z, Adeoye O.O, Adetola B.A. 2004. Geoelectrical investigation of the Ondo State

Housing Corporation Estate, Ijapo Akure, Southwestern Nigeria. J Min Geol 40(1):41–48 Google Scholar

Olorunfemi M.O. 2001. Geophysics as a tool in Environmental Impact Assessment, NACETEM, Obafemi Awolowo University, Ile Ife, Course on Environmental Impact AssessmentGoogle Scholar

Omosanya K.O, Akinmosin A, Balogun J. 2014. A review of stratigraphic surfaces generated from multiple electrical sounding and profiling. RMZ Mater Geoenviron 61(1):49–63 Google Scholar

Omosuyi G.O, Ojo J.S, Olorunfemi M.O. 2008. Geoelectric sounding to delineate shallow aquifers in the coastal plain sands of Okitipupa Area, Southwestern Nigeria. Pacific J Sci Technol 9(2):562–577Google Scholar

Palacky G.J. 1988. Resistivity characteristics of geologic targets. In: Nabighian MN (ed) Investigations in geophysics, vol 3: electromagnetic methods in applied geophysics-theory, vol 1. Society of Exploration Geophysicists, Tulsa, pp 53–129 Google Scholar

Rosqvist H, Dahlin T, Fourie A, Rohrs L, Bengtsson A, Larsson, M. 2003. Mapping of leachate plumes at two landfill sites in South Africa using geoelectrical imaging techniques. In: Proceedings of the 9th international waste management and landfill symposium, Cagliari, Italy, pp 1–10 Google Scholar

Ugwu, S. A., and Nwosu, J. I. 2009. Detection of Fractures for Groundwater Development in Oha-Ukwu using electromagnetic profiling. J.App. Sci. Environ. Manage. Vol.13 (4) 59-63.

Van Stempvoort D, Ewert L, Wassenaar, L. 1992. Aquifer vulnerability index: a GIS-compatible method for groundwater vulnerability mapping. Can Water Resour J 18:25–37 CrossRef Google Scholar

Van Stempvoort, D, Ewert, L and Wassenaar, L. 1993. Aquifer vulnerability index: A GIS compatible method for groundwater vulnerability mapping, Canadian Water Resources Journal 18, pp. 25–37.

Vander Velpen B.P.A. 1988. RESIST version 1.0 M.Sc. Research Project ITC, Deft, Netherlands Google Scholar

Vereecken H, Hubbard S, Binley A, Ferre T. 2004. Hydrogeophysics: an introduction from the guest editors. Vadose Zone J 3:1060–1062Google Scholar

WAPCO. 2000. Environmental Audit Report of the West African Portland Cement Plc, Ewekoro and Shagamu Quarries Submitted To the Federal Ministry of Environment, Abuja by the West African Portland Cement Plc, Elephant House, Alausa-Ikeja Lagos, Nigeria. Pp 1-155

WAPCO. 2001. Environmental Impact Assessment Of The Proposed Clinker Line Of The West African Portland Cement Plc, At Ewekoro Submitted To The Federal Ministry Of Environment, Abuja By The West African Portland Cement Plc, Elephant House, Alausa-Ikeja Lagos, Nigeria. Pp 1-155.

Woakes M, Rahaman M.A, Ajibade A.C. 1987. Some metallogenetic features of the Nigerian basement. J Afr Earth Sci 6:655–664 Google Scholar

Zwahlen, F. 2004. Vulnerability and Risk Mapping for the Protection of Carbonate (Karst) Aquifers, Final Report COST action 620: European Commission, Brussels